

RICE UNIVERSITY

The zebrafish maternal factor *pollywog* is required for yolk  
syncytial layer morphogenesis

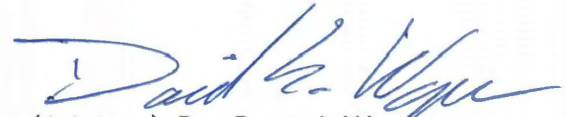
The work of

Christopher Koch Holterhoff

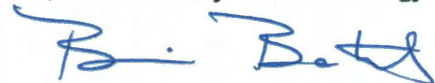
A thesis submitted in partial fulfillment of the requirements for the  
degree

Doctor of Philosophy

Approved, Thesis Committee:



(Advisor) Dr. Daniel Wagner  
Assistant Professor, Biochemistry & Cell Biology



(Chair) Dr. Bonnie Bartel  
Ralph and Dorothy Looney Professor, Biochemistry & Cell Biology



Dr. Michael Stern  
Professor, Biochemistry & Cell Biology



Dr. Michael Kohn

Associate Professor, Ecology & Evolutionary Biology

Houston, Texas  
December 2011 Graduation

## Abstract

In teleosts, the Yolk Syncytial Layer (YSL) is functionally similar to the anterior visceral endoderm found in mice and is required for morphogenesis of the overlying blastoderm. The YSL undergoes dramatic reorganization during early development through processes that mirror the morphogenetic movements of the blastoderm. The YSL and YSL nuclei (YSN) undergo epiboly, and during convergence and extension movements of the blastoderm, the YSN underneath the animal cap also converge and extend underneath the axial hypoblast. Our work with *pollywog* (*pwg*) maternal-effect mutants highlights the delicate control of the YSL during yolk morphogenesis, and provides novel insight into understanding which tissues of the embryo are affected by loss of a cohesive YSL. I found that *pollywog* encodes the zebrafish *mitogen activated protein kinase kinase kinase 4* (*map3k4*) gene and that it acts upstream of *p38a* MAPK in the YSL. I show that this pathway acts in the YSL along with a mixer gene family member, *mix-type homeobox gene 1* (*mxtx1*), to non-autonomously coordinate extracellular matrix deposition and morphogenetic movements in the overlying blastoderm. Our data describes an early and novel role for Map3k4, p38a and Mxtx1 activity that is required for proper morphogenesis of the YSL and the blastoderm. In embryos lacking maternal Map3k4, the YSL undergoes a rapid and catastrophic retraction and the YSN lose their normal distribution around the yolk. The prechordal plate of *pwg* mutant embryos deflect laterally or plunge into the yolk, and the overall animalward extension of the prechordal plate is diminished. I also show that the anterior neural plate of *pwg* mutant embryos

fail to converge dorsally to the same extent as in wild embryos. These data show that the p38 MAPK pathway is essential for maintaining normal yolk cell equilibrium during early development and that without proper cues from the YSL, the blastoderm cannot complete its morphogenetic movements.

Included in this thesis is work highlighting the alpha-actinin gene family in zebrafish. alpha-actinins are actin microfilament crosslinking proteins. Vertebrate actinins fall into two classes: the broadly-expressed *actinins* 1 and 4 (*actn1* and *actn4*) and muscle-specific actinins, *actn2* and *actn3*. Members of this family have numerous roles, including regulation of cell adhesion, cell differentiation, directed cell motility, intracellular signaling and stabilization of f-actin at the sarcomeric Z-line in muscle. Here I identify five zebrafish actinin genes including two paralogs of *ACTN3*. I describe the temporal and spatial expression patterns of these genes through embryonic development. All zebrafish actinin genes have unique expression profiles, indicating specialization of each gene. In particular the muscle actinins display preferential expression in different domains of axial, pharyngeal and cranial musculature. There is no identified avian *actn3* and approximately 16% of humans are null for *ACTN3*. Duplication of *actn3* in the zebrafish indicates that variation in *actn3* expression may promote physiological diversity in muscle function among vertebrates.

## Acknowledgements

"Stay, my lord,  
And let your reason with your choler question  
What 'tis you go about: to climb steep hills  
Requires slow pace at first..."

Duke of Norfolk, *HENRY VIII*, W. Shakespeare

I would first like to recognize my advisor and friend, Dan Wagner. It has been humbling to have such a knowledgeable advisor. His constant willingness to instruct and further my own development both in and out of the lab is a credit to Rice University and this department. My years spent under his instruction have resulted in a profound clarity, both professionally and personally, for which I am simply and extremely grateful.

I would also like to enthusiastically thank my former committee Chair, Mary Ellen Lane, who has moved on from Rice. Sincere and candid with me always, she provided input on my projects as well as advice without hesitation in all things that I asked, as well as some things that I did not think to ask. Likewise with the rest of my committee members: Drs. Bonnie Bartel, Michael Stern, Cindy Farach-Carson and Michael Kohn. I still remember how pleased I was upon your appointments to this committee, and am thankful for your unwillingness to accept mediocrity and insist upon quality always.

It is amazing how heritable traits interact with each other, and I am bewildered to find in myself unique aspects of both my parents, Frank and Mary. I hope that I will make you proud as I continue onward; your respect is a great reward, even if I don't call often enough.

Finally, I dedicate my small work, such as it is, *ad maiorem Dei gloriam*. Though I use my abilities to tease apart the smallest and most delightfully cunning mechanisms of Thy creation, and lo! gravity's cruel force conspire along with poor posture to keep my head bowed, may my *splenius capitem* never atrophy from lack of exercise, that I may not lose the magnitude for the minutiae.

## Table of Contents

<b>Abstract</b> .....	<b>ii</b>
<b>Acknowledgements</b> .....	<b>iv</b>
<b>Table of Contents</b> .....	<b>v</b>
<b>List of Figures and Tables</b> .....	<b>viii</b>
<b>List of Abbreviations</b> .....	<b>x</b>

### **CHAPTER 1: Background**

1.1	Significance .....	1
1.2	<i>pwg</i> is a novel maternal-effect mutation .....	2
1.3	Morphogenesis results in the vertebrate body plan.....	2
1.4	Identity and behavior of the prechordal plate.....	4
1.5	Morphogenesis and cytoskeletal elements of the YSL.....	6
1.6	Signals from the YSL influence morphogenesis and ECM deposition in the embryo proper .....	8

### **CHAPTER 2: Materials and Methods**

2.1	Fish care.....	10
2.2	In situ probe cloning and in situ hybridization.....	10
2.3	Histology.....	11
2.4	Alpha-actinin gene sequencing.....	12
2.5	Accession numbers for actinin genes.....	12
2.6	Sequence analysis.....	13
2.7	RT-PCR.....	13

2.8	Immunohistochemistry.....	14
2.9	Injection of morpholino antisense nucleotides .....	14
2.10	Mapping and cloning of <i>pwg</i> .....	15
2.11	Embryo analysis.....	15

### CHAPTER 3: Results

3.1	<i>pollywog</i> mutants display defects in embryonic morphogenesis.....	17
3.2	<i>pwg</i> mutant embryos display defective convergence extension and anterior migration of the prechordal plate.....	19
3.3	<i>pwg</i> mutants have defective ECM deposition.....	23
3.4	Dominant negative <i>p38a</i> MAPK recapitulates the <i>pwg</i> phenotype.....	26
3.5	<i>pwg</i> is required for normal yolk morphogenesis.....	28
3.6	<i>mxtx1</i> genetically interacts with <i>pwg</i> to regulate yolk integrity.....	30
3.7	<i>pwg</i> encodes the zebrafish <i>map3k4</i> .....	36
3.8	<i>gadd45beta-b</i> , a possible upstream activator of <i>map3k4</i> .....	43

### Chapter 4: The alpha-actinin gene family

4.1	Brief statement from the author.....	45
4.2	Introduction.....	45
4.3	Identification of zebrafish alpha-actinin homologs.....	49
4.4	Temporal expression profile of zebrafish alpha-actinin genes.....	54
4.5	Tissue specific expression of zebrafish actinins.....	56
4.6	<i>actn1</i> and <i>actn4</i> : the non-muscle actinins.....	56

4.7	<i>actn2</i> , <i>actn3a</i> , <i>actn3b</i> : the muscle actinins during axial muscle development.....	60
4.8	Muscle actinins display different patterns of expression in the pharyngeal and cranial muscles.....	66
4.9	Differential expression of <i>actn2</i> in mandibular and hyoid arches.....	66
4.10	Differential expression of <i>actn3</i> paralogs in branchial arches and somite-derived anterior muscles.....	67
4.11	Expression of <i>actn2</i> , <i>3a</i> and <i>3b</i> in the sternohyoideus muscles.....	70
4.12	Conclusion.....	71

## **Chapter 5: Discussion**

5.1	<i>pwg</i> regulates YSL integrity during morphogenesis .....	74
5.2	Conditional interactions between <i>map3k4</i> , <i>mxtx1</i> and <i>fibronectin</i> .....	75
5.3	Role of YSL during morphogenesis.....	76
5.4	Future work.....	78

<b>CHAPTER 6: Works Cited.....</b>	<b>81</b>
------------------------------------	-----------

## List of Figures and Tables

Figure 1.1.	Dorsal drawing of 60% epiboly embryo.....	5
Figure 3.1	Overview of 24hpf <i>pwg</i> phenotype.....	18
Figure 3.2	<i>pollywog</i> embryos display defective extension of axial mesoderm as well as defective dorsal convergence of the anterior neural plate.....	20
Figure 3.3	ECM deposition is decreased in <i>pwg</i> mutants.....	24
Figure 3.4	Injection of dominant-negative <i>p38a</i> RNA into wild type embryos recapitulates the <i>pwg</i> phenotype.....	27
Figure 3.5	<i>pwg</i> embryos undergo rapid and catastrophic loss of YSL integrity.....	29
Figure 3.6	<i>mxtx1</i> genetically interacts with <i>pollywog</i> .....	32
Figure 3.7	<i>fn1</i> morpholino injected into <i>pwg</i> embryos causes cardia bifida but does not increase the penetrance of the <i>pwg</i> phenotype.....	34
Figure 3.8	<i>pwg</i> encodes the zebrafish <i>map3k4</i> .....	37-38
Figure 3.9	<i>mxtx1</i> expression is retained in <i>pwg</i> mutant embryos .....	42
Figure 3.10	Morpholino knockdown of <i>gadd45bb</i> possibly recapitulates the <i>pwg</i> phenotype.....	44
Figure 4.1	The zebrafish genome contains 5 alpha-actinin genes.....	51
Figure 4.2	Temporal expression profiles of zebrafish actinins as shown by semi-quantitative PCR.....	55



Figure 4.3	Expression of the actinin gene family at 24-48 hpf.....	57
Figure 4.4	Muscle-specific actinins are differentially expressed in axial and craniofacial musculature at 96 hpf.....	63
Table 4.1	Relative expression of muscle actinins in 96 hpf cranial and pharyngeal muscles.....	69

## List of Abbreviations

<i>actn</i>	alpha actinin (1-4)
<i>bbp</i>	<i>betty boop</i>
ECM	extracellular matrix
<i>fn</i>	<i>fibronectin1</i>
<i>hgg1</i>	<i>cathepsin L, 1 b</i>
hpf	hours post fertilization
ISH	<i>in situ</i> hybridization
<i>In</i>	<i>laminin</i>
MAPK	mitogen activated protein kinase
<i>map3k4</i>	<i>mitogen activated protein kinase kinase kinase 4</i>
MBT	mid-blastula transition
<i>mk2</i>	<i>mitogen activated protein kinase activated protein kinase 2 (mapkapk2)</i>
<i>myhz2</i>	<i>myosin, heavy polypeptide 2, fast muscle specific</i>
<i>mxtx</i>	<i>mix-type homeobox gene (1 or 2)</i>
<i>nkx2.5</i>	<i>NK2 transcription factor related 5</i>
<i>ntl</i>	<i>no tail</i>
<i>otx2</i>	<i>orthodenticle homolog 2</i>
<i>pax2.1</i>	<i>paired box gene 2a</i>
PPL	prechordal plate
<i>pwg</i>	<i>pollywog</i>
RT-PCR	reverse transcription polymerase chain reaction
<i>shh</i>	<i>sonic hedge hog</i>
<i>sox19a</i>	<i>SRY-box containing gene 19a</i>
<i>stnnc</i>	<i>troponin C type 1b</i>
YSL	yolk syncytial layer
YSN	yolk syncytial nuclei

## Musculature Abbreviations (also found in Table 4.1)

am	adductor mandibulae	rc	rectus communis
do	dilator operculi	rv	rectus ventralis
ima	intermandibularis anterior	tv	transversus ventralis (1-5)
imp	intermandibularis posterior	io	inferior oblique
lap	levator arcus palatini	ir	inferior rectus
ah	adductor hyoideus	lr	lateral rectus
ao	adductor operculi	mr	medial rectus
hh	hyohyoideus	so	superior oblique
ih	interhyoideus	sr	superior rectus
lo	levator operculi	sh	sternohyoideus
dpw	dorsal pharyngeal wall (1-5)		

## CHAPTER 1: BACKGROUND

### 1.1 Significance

Execution of the vertebrate genetic program during early development is heavily dependant upon maternal factors deposited into the developing oocytes prior to fertilization. Maternally derived mRNA and proteins provide the developing animal with an initial organization and context in which the animal's own genome can produce a coherent set of instructions once zygotic transcription is initiated. Maternal factors provide nutrition, directing development until the onset of zygotic transcription and provide a framework to direct the initiation of zygotic transcription. In *Danio rerio*, this initiation is concomitant with the Mid-Blastula Transition (MBT) and is soon followed by the onset of morphogenetic movements. Maternal factors also persist after the MBT and interact with newly synthesized zygotic factors. Morphogenesis then results in the highly organized vertebrate body plan in an orchestrated effort between maternal and zygotic factors.

Zygotic screens have isolated a wide array of mutations in zebrafish that affect morphogenesis and embryonic development (Driever et al., 1996; Haffter et al., 1996; Hammerschmidt et al., 1996; Kane et al., 1996). However, zebrafish development is extraordinarily rapid and large gaps remain in the knowledge base of developmental processes. Existing mutational genetic analysis gained from zebrafish as well as other vertebrate models fails to account for many key developmental processes that have

been observed. It was hypothesized that a maternal-effect screen would uncover additional genes necessary for development (Pelegri and Schulte-Merker, 1999). *pollywog* was discovered in one of these screens (Dosch et al., 2004; Wagner et al., 2004).

Because many important aspects of morphogenesis are conserved across the vertebrate family, elucidation of these genetic pathways will allow for a better understanding of human development and related pathology.

## **1.2 *pwg* is a novel maternal-effect mutation**

Homozygous *pwg* mutant females show no observable phenotype during development or adulthood. When crossed to wild type males, their offspring display an unusual anterior morphogenetic defect (described in detail in RESULTS), indicating that maternal *pwg* is necessary for normal development. Since this is a maternal effect mutation, all experiments described are performed by mating homozygous mutant females to wild type males. Embryos are genetically heterozygous for the *pwg* locus, but lack a necessary maternal factor from the mother and display the mutant phenotype and so are referred to as *mutant embryos* despite being heterozygous.

## **1.3 Morphogenesis results in the vertebrate body plan.**

Following expansion from a single cell into a multi-celled blastoderm at the animal pole of the embryo, three general morphogenetic movements create a recognizable body plan. First, *epiboly* brings the cells down around

the surface of the yolk, eventually enveloping the yolk cell (downward arrows in Fig. 1.1). During normal development at roughly 50% through epiboly, cells at the leading margin begin to *involute* and travel back towards the animal pole along the overlying cells, creating an inner cell layer of mesendodermal cells (the hypoblast), and an outer layer of neural and non-neural ectoderm (the epiblast; rounded arrows in Fig. 1.1; (Kimmel et al., 1995; Montero and Heisenberg, 2004). Finally, *convergence and extension* (CE) movements bring more lateral cell populations closer to the axial midline, accomplishing both a thickening of dorsal tissues along the anterior-posterior axis and, through medio-lateral intercalation, an extension along the main axis (upward arrow in Fig 1.1). Glickman *et al.* (2003) have shown that convergence and extension behaviors may be disparate activities; *no tail* mutants in which medial mesendodermal cells do not intercalate and fail to converge normally still have extension in some axial tissues. This raises the possibility that at least part of the anterior-posterior extension of the involuted cells is the result of migratory behavior under control of different factors, or these movements could be regulated by a parallel pathway. It should be noted that all cell types (endo- meso- and ectodermal cells as well as overlying yolk syncytial layer (YSL) nuclei) display axial convergence in the developing zebrafish (Warga and Kimmel, 1990; D'Amico and Cooper, 2001). This means that both involuted and non-involuted cells and YSL nuclei dynamically reorganize towards the midline during gastrulation (roughly from 50% epiboly through to early somite stages). Following these movements, inductive signals from cell

populations brought adjacent to each other by these movements are then able to pattern tissues correctly and modulate cell motility.

#### **1.4 Identity and behavior of the prechordal plate (PPL)**

Because the *pwg* mutant phenotype as described below involves aberrancies in PPL migration or specification, a short explanation as to the morphology and possible function of the PPL is necessary. The cells that involute first at the dorsal thickening (shield) form the anterior tissues of the midline mesoderm (also herein referred to as axial mesoderm). These cells are anterior to the notochord and therefore referred to as the prechordal plate (Fig. 1.1) and around shield stage contain mRNA of maternal or zygotic origin encoding *gooseoid* as well as BMP and Wnt signal antagonists *chordin* and *dikkopf1*, respectively, as well as *cyclops*, which is involved in nodal signaling (for a review see (Kimelman and Schier, 2002)). At the very extreme leading edge of PPL cells, filopodial and lamellapodial cellular processes preferentially extend outward in the vector orientation of anterior extension. It is thought that these extensions play an important role in the forward (animal-ward) migration of the anterior PPL cells through E-cadherin and Fibronectin-mediated cell-ECM and cell-cell adhesion and communication (Montero et al., 2005). In *silberblick/wnt11* mutants, the anterior PPL cells do not show oriented filopodia aligned true to their migrational vector and do not migrate as far as wild type controls (Ulrich et al., 2003). This would suggest that an accurate control of cell extension is

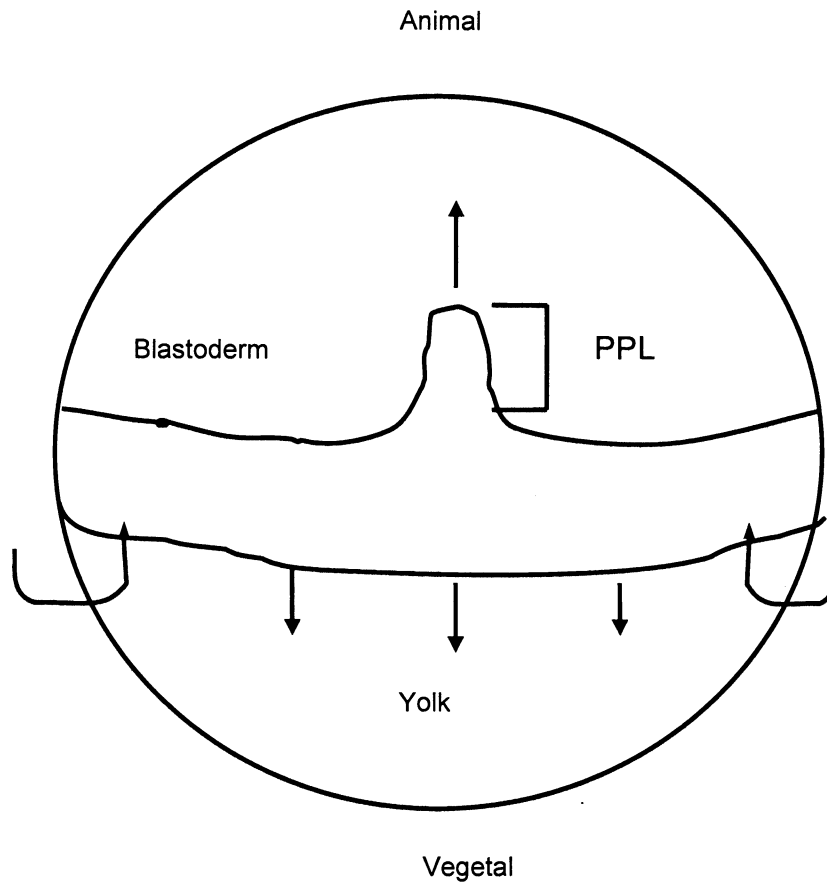


**Figure 1.1.** Schematic of a 60% epiboly embryo viewed from dorsal. The prechordal plate (PPL) cells are the leading and most anterior of the involuted mesendodermal cells. Arrows indicate morphogenetic movements: epiboly, involution, convergence and extension.

needed for proper anterior movement of the PPL. One of the pathways utilized by PPL cells to regulate their cellular extensions is PI3K signaling. When PI3K signaling is perturbed, PPL cells fail to successfully migrate to their anterior destination and display significantly fewer normal cell extensions (Montero et al., 2003). This PI3K regulation suggests similarities of PPL migrational behavior to other conserved cell migration and chemotactic responses and raises the exciting possibility that understanding any role *pwg* has in regulating or potentiating these cell migratory behaviors could give insight into the mechanics of dynamic cell migration in cancer, immune response or tissue repair systems.

### **1.5 Morphogenesis and cytoskeletal elements of the YSL**

While these morphogenetic movements establish the teleost embryo proper, in all teleosts, a syncytium is formed from the blastomeres that are most proximal to the yolk during cleavage (Carvalho and Heisenberg, 2010). This yolk syncytial layer (YSL) is an extra-embryonic structure required for numerous processes central to development, including epiboly, mesendoderm specification of the blastoderm from yolk Nodal/TGF- $\beta$  activity (Mizuno et al., 1996; Ober and Schulte-Merker, 1999), migration of heart precursor cells during organogenesis (Arrington and Yost, 2009; Kawahara et al., 2009; Osborne et al., 2008; Sakaguchi et al., 2006), and regulation of metabolite access during this intense period of growth (Marza et al., 2005). Interestingly, the teleost-specific YSL is functionally similar to the mouse anterior visceral endoderm (AVE), an extra-embryonic tissue. For example,



signals originating in both the AVE and YSL regulate canonical WNT and Nodal signaling to pattern the embryo proper, and the expression of the zebrafish *hhex* homologue in the YSL and its role in anterior fate specification is similar to its expression and role in the AVE (Bischof and Driever, 2004; Rodriguez et al., 2005).

Tracking movement of the yolk syncytial nuclei (YSN) reveals the dramatic reorganization of the yolk cell that closely resembles the morphogenetic movements of the overlying blastoderm. YSN underneath the animal cap dorsally converge and extend towards the animal pole during gastrulation, while the marginal YSN that underlie the blastoderm margin undergo epiboly (D'Amico and Cooper, 2001). Disruption of the YSL by injecting RNase into the YSL compartment of pre-gastrulating embryos results in failure to correctly specify ventrolateral mesendoderm (Chen and Kimelman, 2000). Furthermore, these embryos fail to complete epiboly, and shortly after 50% epiboly, the blastoderm detaches from the yolk resulting in embryonic death. Disruption or stabilization of the YSL microtubules by treatment with nocodazole or taxol, respectively, alters epiboly progression and alters development (Solnica-Krezel and Driever, 1994). Thus, structural stability via cytoskeletal elements is required in the YSL during development.

## 1.6 Signals from the YSL influence morphogenesis and ECM deposition in the embryo proper

An emerging body of data has provided new appreciation for the yolk cell's role in morphogenesis of the overlying blastoderm. Recent work has shown the requirement of signals from the YSL to regulate extracellular matrix deposition in the embryo proper. By knocking down the *mix-type homeobox gene 1 (mxtx1)* specifically in the YSL, the ECM components normally associated with the polarized lateral plate mesoderm were absent or greatly reduced, and similar to *natterlfibronectin1 (fn1)* mutants, heart precursor cells fail to migrate to the midline to form the heart tube (Trinh and Stainier, 2004). It was also shown that Fn1 protein, although expressed and secreted in monomeric form in the blastoderm, is regulated by *mxtx1* non-autonomously from the YSL (Hirata et al., 2000; Sakaguchi et al., 2006; Trinh and Stainier, 2004). It has been proposed that *mxtx1* is required for proper activation of sphingolipid transport and receptor activation from the YSL, which could influence cell motility and adhesion (Carvalho and Heisenberg, 2010; Kai et al., 2008; Kawahara et al., 2009; Osborne et al., 2008). Other factors expressed in the YSL, such as *Syndecan2*, play a role in ECM maturation and fibrillogenesis and are required for morphogenesis in a seemingly separate genetic pathway (Arrington and Yost, 2009). This elaborate system of ensuring a suitable ECM environment for organogenesis is further influenced by the cardiac precursor cells themselves, which express genes such as *hand2*, a basic-Helix-Loop-Helix transcription factor that can inhibit

Fibronectin1 fibrillogenesis non-autonomously (Garavito-Aguilar et al., 2010). Another, related gene from the mix-type family of homeobox genes, *mxtx2*, is expressed in the YSL and is important for filamentous actin remodeling during epiboly, but has no described role in promoting ECM deposition (Bruce et al., 2005; Hirata et al., 2000; Wilkins et al., 2008).

## **Chapter 2: Materials and Methods**

### **2.1 Fish care**

All fish maintenance was performed according to Rice University and NIH animal care procedures. Embryos were collected and reared at 28°C in E3 embryo media. Optionally, to eliminate pigmentation after 24 hpf, 1-phenyl-2-thiourea (PTU) was added to the E3 fish media at 0.003% (w/v) to inhibit melanin production. All staging was performed as described (Kimmel et al., 1995).

### **2.2 in situ probe cloning and in situ hybridization**

For construction of anti-sense riboprobe suitable for *in situ* hybridization, zebrafish target cDNAs were amplified with the high fidelity Phusion polymerase (Finnzymes/New England Biolabs, F-530L) and cloned into pGEM-T EZ vector (Promega, #A1360). *myhz2* plasmid was obtained from ZIRC (CB-38) Zebrafish International Resource Center (ZIRC). *in situ* probes obtained were *hgg1* (Thisse et al., 1994), *shh* (Krauss et al., 1993), *pax2.1* (Krauss et al., 1992), *dlx3* (Akimenko et al., 1994), *ntl* (Schulte-Merker et al., 1994), *sox19a* (Thisse et al., 2001), *nkx2.5* (Lee et al., 1996), *otx2* (Li et al., 1994), *mxtx1* (Hirata et al., 2000).

In order to compensate for the high degree of relatedness among the zebrafish alpha-actinins, where possible, EST data obtained from the zebrafish Ensemble Genome Browser (Wellcome Trust Sanger Institute) that yielded 3' UTR sequence (verified through NCBI BLAST searches) was

targeted in conjunction with coding sequence for cloning to ensure probe specificity for each zebrafish  $\alpha$ -actinin gene.

Whole mount *in situ* hybridization staining was done essentially as described (Schulte-Merker et al., 1994; Thisse et al., 1993). Embryos and larvae were manually dechorionated and treated with 0.04% Tricaine (Sigma) prior to fixation in 4% (*w/v*) paraformaldehyde. Fixed embryos aged 24, 36 or 48 hpf were treated with ProteinaseK (Fisher) at a concentration of 10  $\mu$ g/ml in phosphate buffered saline with 0.1% Tween-20 for 5, 10 or 15 minutes, respectively. Stained embryos and larvae were semi-permanently whole mounted in GMM (10% (*v/v*) methyl salicylate (Sigma, M-6752) in Canada balsam (Sigma, C-1795) for imaging. Photomicrographs were obtained using an AxioCam MRc5 camera (Zeiss) mounted on an Axiovert 200M inverted stereomicroscope (Zeiss). The relative expression of *actn2*, *actn3a* and *actn3b* at 96 hpf was determined using either expression in the levator arcus palatine as a reference for high level of expression for all muscles, or comparatively scoring the relative intensities between the three genes for each individual muscle independently. Both scoring methods yielded similar results.

### **2.3 Histology**

For cryosectioning, whole mount stained embryos were equilibrated overnight in a solution of 7.5% sucrose in PBST at 4°C to reduce dehydration

artifacts when samples were later frozen. Embryos were equilibrated for 1 to 6 hours in OCT embedding medium (Sakura Finetek USA, 4583), then oriented in OCT at 25°C, frozen on dry ice, and stored or sectioned at -20 to -25°C. Sections were obtained using a Harris-Cryostat (International Equip. Co., model CTD) at a thickness of 10µm or more and captured on FrostPLUS positively charged glass slides (VWR, 48311). Eosin Y (Sigma) was used to counter stain *in situ* specimens.

#### **2.4 Alpha-actinin gene sequencing**

Full length alpha-actinin genes were PCR-amplified. Overlapping internal primer sets were used for sequencing and can be found in Holterhoff et al., 2009.

#### **2.5 Accession numbers for actinin genes**

A list of actinin sequences used to create the phylogenetic tree in Figure 4.1 can be found in Holterhoff et al., 2009. Zebrafish actinin sequences were identified using a reciprocal BLAST approach. Annotated *Homo sapiens* and *Mus musculus* gene entries for each of the four actinins were used in a BLAST search against the zebrafish genome build (Wellcome Trust Sanger Institute) to identify putative zebrafish homologs. These gene sequences were then queried against the human and mouse genomes to ensure all zebrafish actinin genes were identified.

## **2.6 Sequence analysis**

Alignment of tetrapod alpha-actinins was performed by nearest neighbor joining of the actinin protein sequences or the translations of our sequenced actinins listed in Holterhoff et al. (2009). The zebrafish actinin protein sequences obtained in our analysis were used for this alignment. The alignment and identity of the coordinating amino acids in the EF hands is after Beggs et al., 1992; Tang et al., 2001. Initial synteny conservation was established by searching the Synteny Database (Catchen et al., 2009). Database output was updated from the latest builds of zebrafish and human pseudogenes were removed. Accession numbers for zebrafish loci were updated with gene names from Vega ([http://vega.sanger.ac.uk/Danio\\_rerio/index.html](http://vega.sanger.ac.uk/Danio_rerio/index.html)) or Zv8 ([http://www.ensembl.org/Danio\\_rerio/Info/Index](http://www.ensembl.org/Danio_rerio/Info/Index)). Where no gene identity has been annotated the accession number was used even in cases where the Synteny Database established identity.

## **2.7 RT-PCR**

RNA was prepared from the indicated stages by Trizol lysis and purification (Invitrogen). cDNA was prepared with the ImPromII cDNA synthesis kit (Promega) according to the manufacturer's protocol with the substitution of random pentadecamers for random hexamers. PCR was performed using the primers at appropriate annealing temperatures. The

PCR was conducted for the indicated cycle number, and then the product was analyzed by agarose gel electrophoresis and Ethidium bromide staining. *odc* primers were used to standardize the output for analysis (Draper et al., 2001).

## **2.8 Immunohistochemistry**

Immunohistochemistry was performed as described (Trinh and Stainier, 2004). We used rabbit polyclonal anti-Fibronectin (Sigma) (Trinh and Stainier, 2004) at 1:200; rabbit polyclonal anti-Laminin1 (Sigma) at 1:200. Embryos were cryosectioned and mounted in VectaShield (Vector Laboratories). Flatmounts were performed by de-yolking in PBDT (1%BSA, 0.1% Triton X-100, 1% DMSO in PBS) and mounting in VectaShield mounting media and images were obtained using an AxioCam MRc5 camera (Zeiss) mounted on an Axiovert 200M inverted stereomicroscope (Zeiss).

## **2.9 Injection of morpholino antisense oligonucleotides**

Antisense morpholinos designed to block translation were obtained (Gene Tools, LLC) and injected at 1-cell or 1000-cell stages as indicated. The following morpholinos were used: *map3k4-mo* (5'-TGCATGAATCAGAACATGTCCAGGA-3'), *mxtx1-mo* (5'-cATGTTGCGTCTTCACTGGTGGAAAT-3'; (Sakaguchi et al., 2006), *fn1-mo* (5'- TCACAGGTGCGATTGAACACGCTAA-3'), *lamc1-mo* (5'-TGTGTCCTTTTGCTATTGCGACCTC-3'; (Parsons et al., 2002), *gadd45bb-mo* (5'-GCGTAAGATACTTACAGTAACAAGT-3').



## **2.10 Mapping and cloning of *pwg***

Genomic DNA was obtained from mutant and wild type sibling females, and the *pwg* mutation mapped to a chromosomal position using Simple Sequence Length Polymorphism (SSLP) markers spaced throughout the genome. SSLP markers flanking the mutation were used to genotype individual fish. Fish were generated for fine mapping by crossing heterozygous *pwg* females with homozygous *pwg* males and meiotic recombination events were observed between SSLP markers z9868 and z26404. Genetic distances shown were determined based on meiotic recombination events observed in a mapping panel of 44 females. Full-length candidate genes were PCR-amplified using overlapping internal primer sets to provide double-coverage sequencing data. Following identification of the *pwg* lesion, dCAPS PCR primers (Neff et al., 2002) were used to genotype fish. Following PCR amplification from genomic DNA prepared from tails (Holterhoff et al., 2009; Primer A 5'GGAACCAAGCCAGTGTTTTATCCCAC3'; Primer B 5'ACGCAGCCTCGATCGCTTGAAGGAATT3'), PCR products were digested with EcoRI restriction enzyme and *pwg* mutants identified by uncut DNA products.

## **2.11 Embryo Analysis**

For analysis of *pwg* phenotypes before segmentation stages only clutches with greater than 95% penetrance were used based on scoring of

surviving siblings at 1 day post fertilization (dpf) unless otherwise indicated. Embryos were scored at 24 hpf for presence of flattened heads and misshapen yolks (*pwg*), non-specific deformations (*other*) or no observable phenotypes (*wild type*). Analysis of embryos at segmentation stages or later were separated into *pwg* phenotype or *wild type* for phenotype analysis. Significance of rescue and phenocopy data was shown using Fisher's Exact test. For morphometric analysis, two-tailed t-Test analysis was performed on embryo measurements obtained using AxioVision software (Zeiss).

## Chapter 3: Results

### 3.1 *pwg* maternal mutants display defects in embryonic morphogenesis

At 24 hpf, embryos with mutant phenotype obtained from *pwg* homozygous mutant mothers (hereafter referred to as *pwg* mutant embryos) fail to straighten their tails, display a flattened head with widely spaced eyes, a misshapen yolk and visible yolk globules in the yolk cell (Fig. 3.1A-D). The penetrance of the *pwg* phenotype was variable between matings ranging from <5% to >75% (mean=19.6% penetrance for 41 observed matings), but expressivity of the phenotype was uniform, with no partially affected embryos observed.

I examined anterior tissue organization of the 24 hpf *pwg* mutant larvae by whole mount *in situ* hybridization. *sox19a*, a pan-CNS marker in early larvae, was expressed in *pwg* mutants at 28 hpf in cells spanning the length of the spinal cord and in the hindbrain, midbrain and forebrain, indicating initial specification of the CNS (Fig. 3.1F) occurs normally. Expression of *hgg1* and *shh* at 24 hpf revealed that the hatching gland, which forms from the anterior axial mesoderm, is affected in its position and morphology in *pwg* mutants, whereas wild type larvae form a broad crescent-shaped row of cells anterior to the head, *pwg* embryos show a clumped and uneven field of hatching gland cells (arrows in Fig. 3.1G and H). *shh* expression in the chordamesoderm was observed in all *pwg* larvae (Fig. 3.1H), and the notochord is visible. In *pwg* mutant larvae, *nkx2.5* expression in the cardiac precursor cells showed that the bilateral cardiac fields fail to

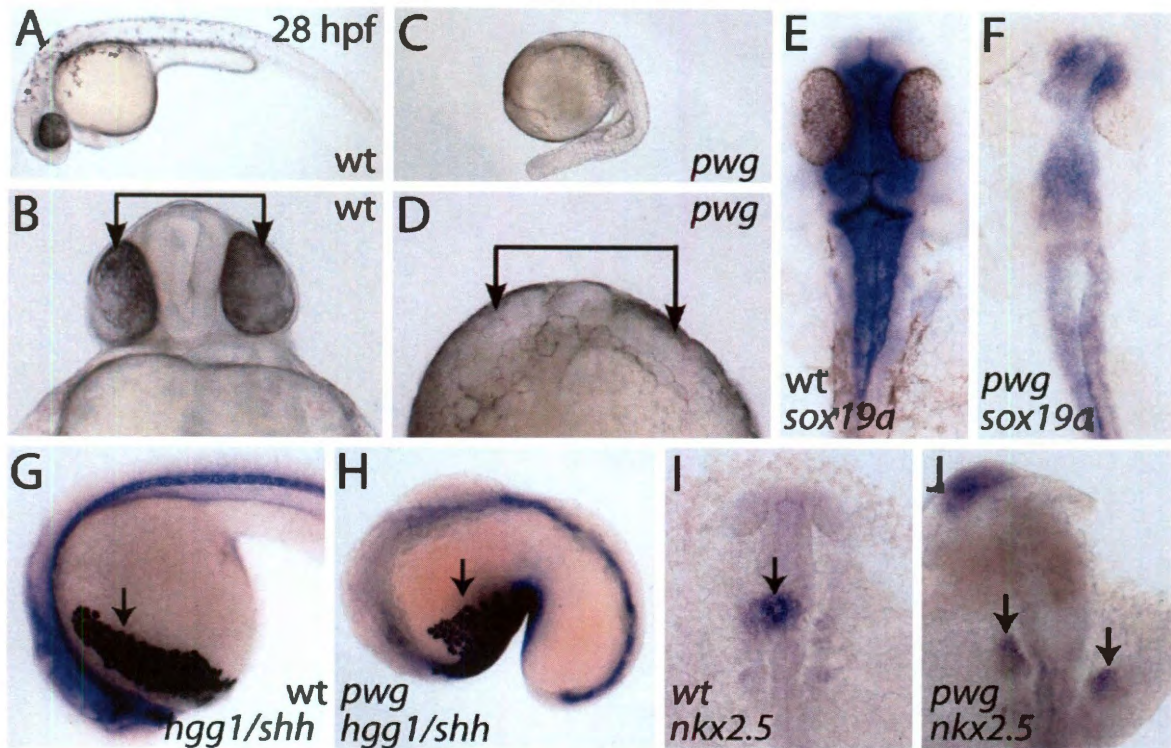


**Figure 3.1.** Characterization of 24-28 hpf *pwg* mutant phenotype morphology. Lateral and frontal whole mount view of wild type (A and B) and *pwg* mutant embryos (C and D) at 28 hpf. Widely set eyes are marked with bracketed arrows in B and D. E and F: flatmount views of *sox19a* expression in wild type (E) and *pwg* mutant (F) embryos at 28 hpf. G and H: lateral view of double *in situ* hybridization for *hgg1* and *shh* expression in wild type (G) and *pwg* mutant (H) embryos at 24 hpf. Arrows indicate location of the *hgg1*-positive hatching gland. I and J: flatmount views of *nkx2.5* expression in wild type (I) and *pwg* mutant (J) embryos at 24 hpf. Arrows indicate location of myocardial precursor cells in I and J.

migrate and fuse to form a single heart tube by 24 hpf (Fig. 3.1I and J), indicating *pwg* embryos are delayed in cardiac organogenesis. For all markers tested in unaffected escaper *pwg* larvae, expression was indistinguishable from wild type embryos, indicating loss of *pwg* results in a bimodal phenotype with no obvious intermediate phenotype.

### **3.2 *pwg* mutant embryos display defective convergence extension and anterior migration of the prechordal plate**

To examine morphogenesis in *pwg* mutant embryos, I performed whole mount *in situ* hybridization to detect *hgg1*, *pax2.1*, *dlx3* and *shh* expression at the end of gastrulation (10 hpf). In wild type embryos, the *hgg1*-positive prechordal plate cells (comprising the anterior-most axial hypoblast) had migrated from the dorsal margin of the embryo to beyond the anterior border of the overlying neural plate (arrowhead in Fig. 3.2A). In *pwg* mutants the prechordal plate failed to extend beyond the anterior portion of the overlying *dlx3*-positive non-neural ectoderm (arrowhead in Fig. 3.2B). Specification of the midbrain-hindbrain boundary as shown by *pax2.1* expression was unaffected in *pwg* mutants (compare Fig. 3.2A and B). These data indicate that the early patterning of the axial mesoderm, as well as the establishment of neural/non-neural ectoderm domains, occurs in *pwg* mutants. However the axial mesoderm fails to execute proper extension.

Morphometric quantification of gene expression data at the 3 somite stage showed that although tissues associated with the prechordal plate and

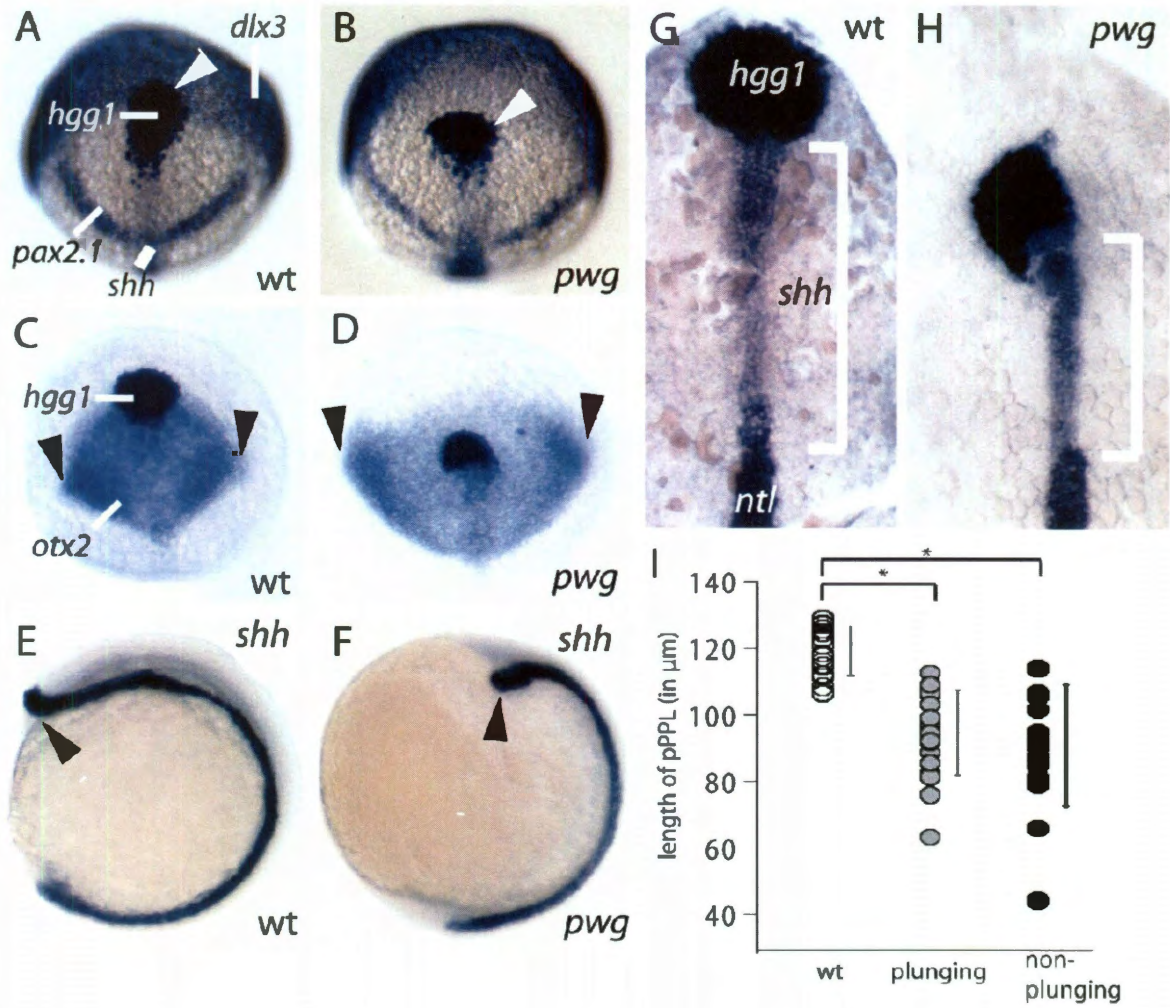


**Fig 3.2** (Figure legend on following page.)

**Figure 3.2.** (Previous page) *pwg* embryos display defective axial mesendoderm extension and anterior neural plate convergence. A and B: animal views of expression of *hgg1* in the anterior prechordal plate, *shh* in the chordamesoderm and posterior neural plate, *pax2.1* expression at the midbrain-hindbrain boundary and *dlx3* expression in the non-neural ectoderm at bud stage wild type (A) or *pwg* (B) embryos. White arrowheads in A and B indicate anterior-most extent of the anterior portion of the prechordal plate. C and D: animal views of expression of *hgg1* in the prechordal plate and *otx2* expression in the anterior neural plate of wild type (C) or *pwg* (D) embryos at bud stage. Black arrowheads in C and D indicate lateral extent of the *otx2*-positive cells of the anterior neural plate. E and F: lateral views at 6 somites of *shh* expression in the chordamesoderm and posterior prechordal plate of wild type (E) or *pwg* (F) embryos. Arrowheads in E and F indicate anterior extent of *shh* expression, which is seen plunging into the yolk in *pwg* embryos (F). G and H: flatmount views of *hgg1* expression in the anterior prechordal plate, *shh* in the posterior prechordal plate and *ntl* expression in the chordamesoderm at 3 somites in wild type (G) or *pwg* mutant (H) embryos. White brackets in G and H indicate tissues measured in I. I: Morphometric display of measure posterior prechordal plate lengths in wild type and *pwg* embryos with plunging or non-plunging prechordal plates at 3 somites.

the neural plate are correctly specified and maintained following dorsal convergence, these tissues do not elongate or converge dorsally, respectively, to the extent observed in wild type embryos. Specifically, I observed that the *shh*-positive, *hgg1*-negative posterior prechordal plate segments were overall significantly shorter in *pwg* mutant embryos than wild type by early segmentation stages (n=20, p-value < 10<sup>-6</sup>), and that this difference in tissue length was significant whether or not the axial mesoderm had plunged into the yolk (Fig. 3.2I; n=20, p-value < 10<sup>-5</sup> for *pwg* embryos with plunging prechordal plates).

*pwg* mutant embryos displayed an anterior neural plate convergence defect. To directly observe dorsal convergence of the anterior neural plate during late gastrulation, we performed *in situ* hybridization to stain for *otx2* expression (Fig. 3.2C and D). In *pwg* mutants with defective prechordal plate migration, the domain of *otx2* expression was laterally broadened when compared to wild type embryos at bud stage (wild type average width = 426 μm vs. *pwg* average width = 519 μm, n = 16, p < 0.0001; measurements indicated by dashed line in Fig 3.2C and D).

This convergence defect was limited to anterior tissues. I probed for *myoD* expression at the 5 somite stage in order to measure the total distance between the lateral extents of the fourth somites in *pwg* mutant and wild type embryos. No significant defects in dorsal convergence in these more



posterior tissues (wild type average somite width = 152  $\mu\text{m}$  vs. *pwg* average somite width = 156  $\mu\text{m}$ ,  $n = 8$ ,  $p > 0.5$ ).

Taken together, the data show that maternal *pwg* regulates anterior migration of the anterior axial mesoderm and dorsal convergence of the anterior neural plate, and that the defect in axial extension occurs whether or not the prechordal plate deflects and plunges into the yolk.

### **3.3 *pwg* mutants have defective ECM deposition**

Knockdown of the zygotically-expressed gene *mxtx1* in the yolk cell of *natter/fibronectin1* heterozygote embryos results in a phenotype similar to *pwg*, with embryos displaying a flattened head, cardia bifida and opaque misshapen yolks (Sakaguchi et al., 2006). In these embryos lacking Mxtx1 function in the yolk, the ECM components of Fibronectin and Laminin were reduced in embryonic tissues. To determine if *pwg* was also required for ECM deposition, I examined Fibronectin1 (Fn1) and Gamma-1-Laminin (LamC1), two components of the early vertebrate ECM (Sakaguchi et al., 2006; Trinh and Stainier, 2004). Immunofluorescence assays using anti-LamininC1 or anti-Fibronectin1 antibodies showed that by 18 hpf, when robust ECM deposition and fibril organization is required for heart organogenesis, *pwg* embryos lacked robust Lam1 or Fn1 deposition as seen in wild type embryos (Fig. 3.3A and B;  $n=7$  for both wild type and *pwg*, representative images shown). The global impact of loss of maternal *pwg* on ECM deposition was apparent in dorsal flat-mount immunofluorescence

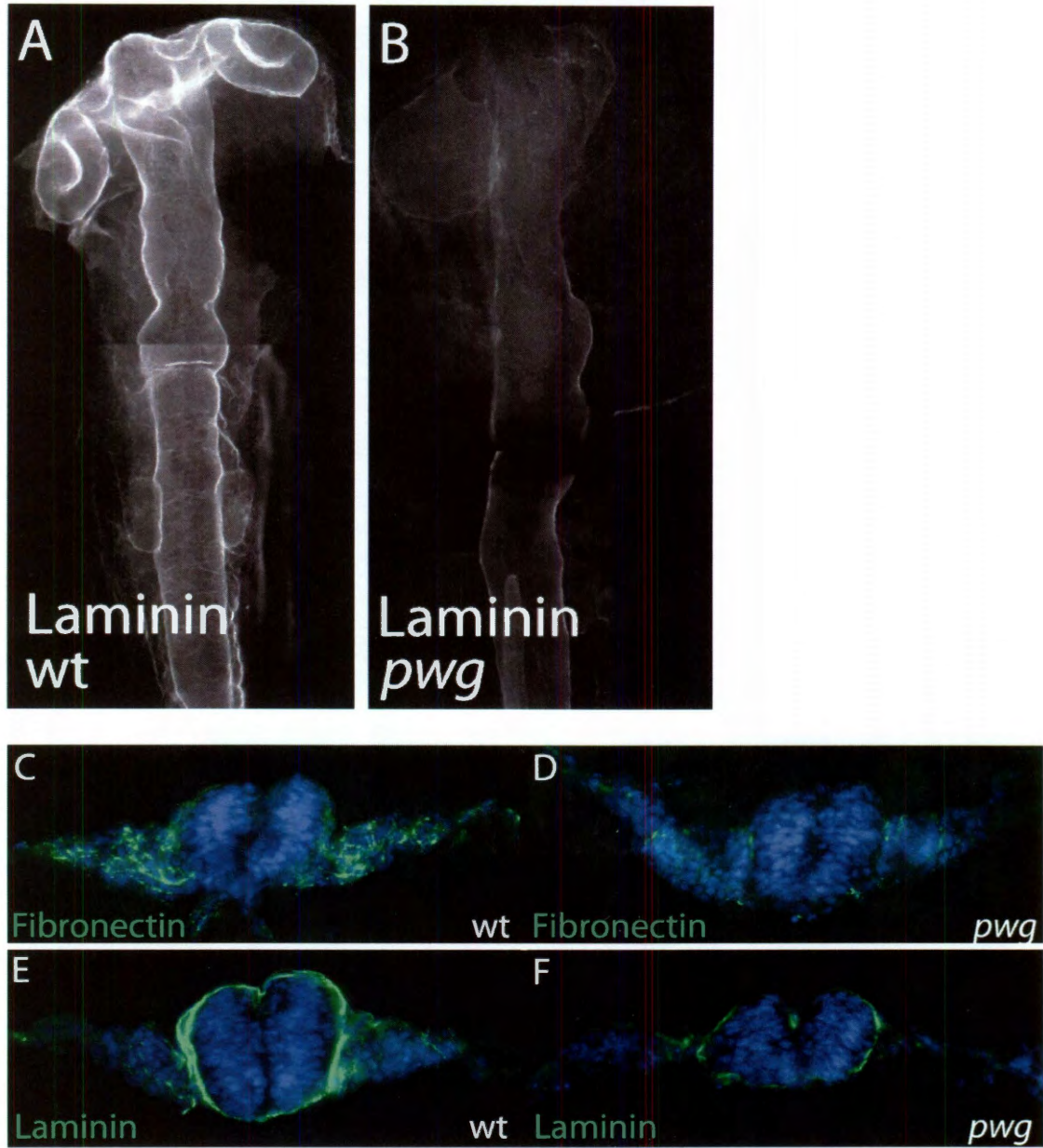


Figure 3.3 (Legend on following page.)

**Figure 3.3** (Previous page) ECM deposition is decreased in *pwg* mutant embryos. A and B: flatmount immunofluorescence images of Laminin deposition in wild type (A) or *pwg* (B) mutant embryos. C-F transverse sections taken at the level of the hindbrain in wild type (C and E) or *pwg* mutant (D and F) embryos. Fibronectin staining shown in C and D; Laminin staining shown in E and F. Both ECM components are shown in green, with DAPI-stained nuclei visible in blue.

assays where Fn1 and LamC1 were greatly reduced around the neural tube along the length of the embryo. Transverse sections at the level of the migrating myocardial cells and anterior lateral plate mesoderm showed that these ECM proteins were also lost in the adaxial cells and lateral mesoderm surrounding the migrating cardiac precursor cells at these stages (Fig. 3.3C-F; n=7 for both wild type and *pwg*, representative images shown). These data indicate that maternal *pwg* is required for general ECM deposition during development.

#### **3.4 Dominant negative *p38a* MAPK recapitulates the *pwg* phenotype**

I observed that microinjection of dominant negative *p38a* (*p38-DN*) RNA at the 1-cell stage or into the yolk syncytial layer phenocopies *pwg* in wild type embryos as well as producing a separate early-lysis phenotype similar to that seen in *betty boop* (*bbp*/ *MAP kinase-activated protein kinase 2*) mutants (Fig. 3.4A and B; (Holloway et al., 2009). In the zebrafish yolk syncytial layer, *p38a*-MAPK acts upstream of MAPKAPK2, a gene disrupted in *betty boop* (*bbp*) mutants (Holloway et al., 2009). In *bbp* mutants, the YSL collapses coincident with a blastoderm margin constriction and yolk lysis at 50% epiboly. Injection of 150 pg of *p38-DN* RNA into wild type embryos resulted in approximately half of the embryos displaying the yolk cell bursting phenotype typical of *bbp* mutant embryos (48%, n=178). By 20 hpf, about half of the survivors displayed flattened heads that failed to elevate off of the

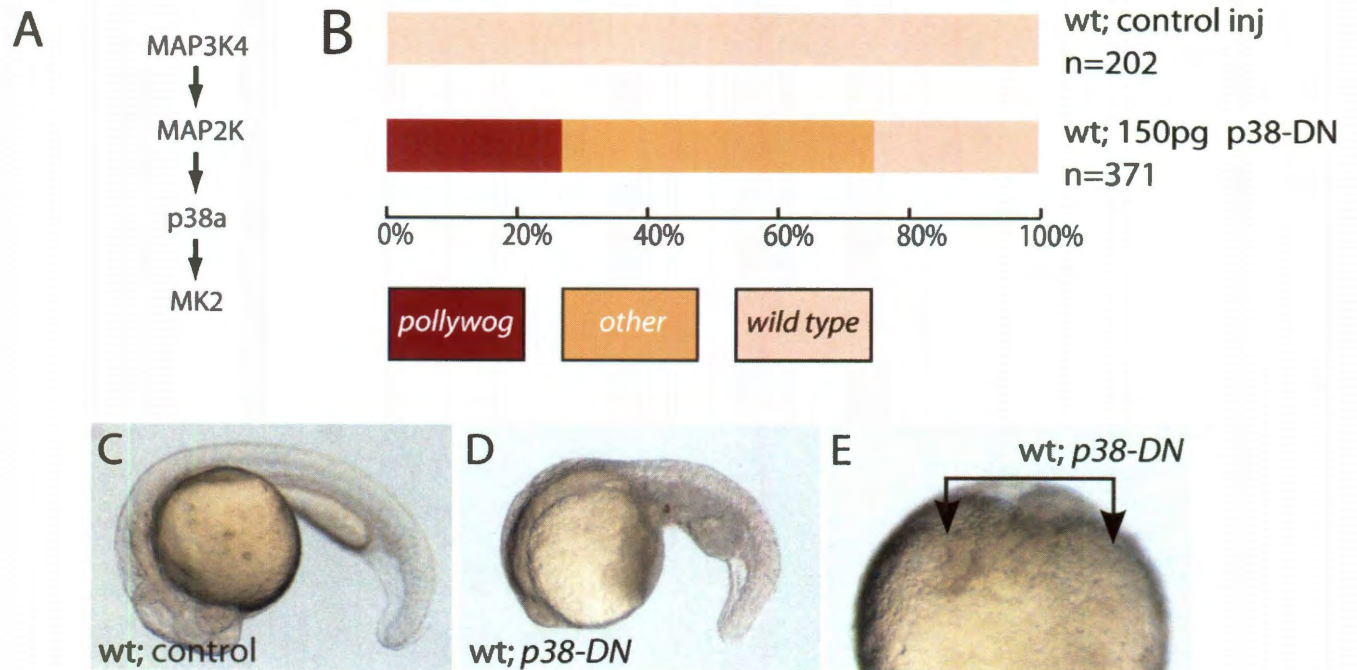


**Figure 3.4** Injection of dominant-negative *p38a* RNA into wild type embryos recapitulates the *pwg* phenotype. A: diagram of vertebrate p38-MAPK activation cascade. B: phenotype distribution scored at 24 hpf following injection of dominant-negative *p38a* RNA into wild type embryos. n-values for each sample indicated next to graph. C-E: whole mount brightfield images of wild type control (C) or *pwg* phenotype *p38-DN* injected (D and E) embryos at 20 hpf. C and D lateral views; E frontal view. Arrows in E indicate widely spaced eyes and compare directly with observed eye morphology in *pwg* mutants (see Fig. 1D).

yolk, with visible yolk globules similar to the *pwg* phenotype (27%, n=100; Fig. 3.4D and E).

### **3.5 *pwg* is required for normal yolk morphogenesis**

Although *pwg* mutants do not lyse at the onset of gastrulation like *bbp* mutants, they do display abnormal yolks during gastrulation and segmentation, and injection of dominant negative *p38* RNA in wild type embryos phenocopied *pwg* as well as *bbp*. I hypothesized that the primary defect in *pwg* embryos might also originate in the YSL as in *bbp* mutant embryos.

In order to test this hypothesis, I examined the distribution and morphology of the yolk syncytial nuclei (YSN) at 24 hpf in wild type and *pwg* mutants by injecting the vital dye Sytox Green into the YSL of wild type or *pwg* embryos. In wild type embryos, the YSN were observed to be evenly distributed throughout the YSL, both along the yolk ball and in the yolk extension (Fig. 3.5A). In all *pwg* mutant phenotype embryos examined at 24 hpf (n=37 from 2 clutches), the YSN were fragmented, with all nuclear material clumped in a disorganized manner near the posterior of the yolk ball (arrowhead in Fig. 3.5B).

To determine the time of onset and nature of this failure, I observed the YSN from initiation of gastrulation through 24 hpf. I observed that *pwg* mutants undergo a dramatic YSL catastrophe. Initially distributed similarly to wild type embryos, *pwg* YSN suddenly clumped together on one side of the

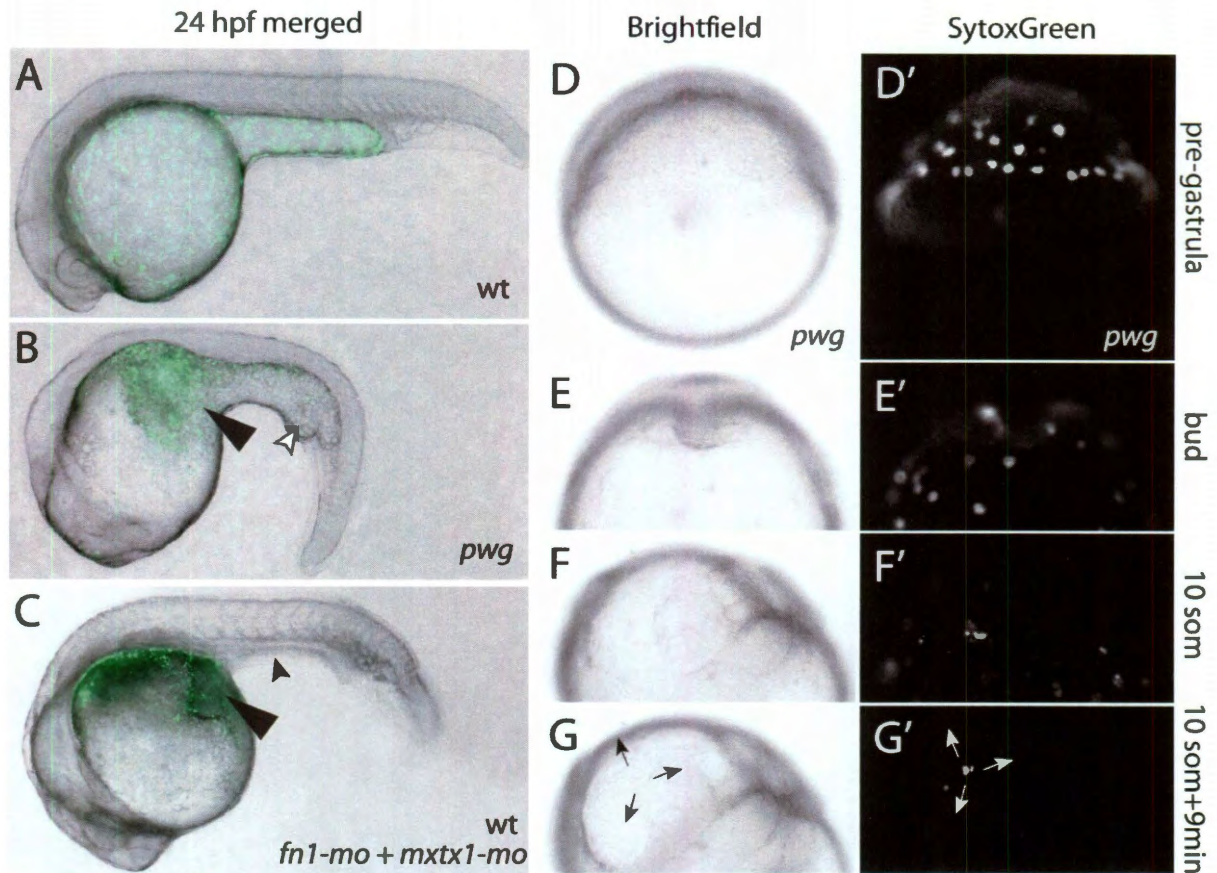


**Figure 3.5.** *pwg* embryos undergo rapid and catastrophic loss of YSL integrity. A-C: lateral views at 24 hpf of Sytox Green-labeled YSN in wild type (A), *pwg* mutant (B) or *fn1/mxtx1* double morphant (C) embryos. Large arrowheads indicate location of nuclear fragments near the posterior region of the yolk ball, white arrowhead indicates visible yolk granules in the mutant embryo, and small black arrowhead indicates lack of yolk extension in the double morphant *pwg* phenocopy. D-G: brightfield time-lapse images of a *pwg* mutant embryo through 14 hours of development. D'-G' green channel images of embryo shown in D-G shows YSN labeling. Arrows in G and G' indicate location of initial YSN retraction and YSL collapse.

embryo within 9-12 minutes of initiation of the YSL collapse (Fig. 3.5D-G). The location of initiation of the YSL snapping varied among *pwg* embryos. Immediately after YSL snapping and retraction, the yolk globules became easily visible, suggesting a mixing of cortical yolk cytoplasm with yolk globules (white arrowhead in Fig. 3.5B).

I also observed that, following YSL catastrophe in *pwg* mutants, the nuclei or nuclear fragments constricted towards the yolk extension (as shown in Fig. 3.5B). This implies that directional forces act on or anchor the YSL during morphogenesis.

This YSL collapse likely disrupts many functions of the yolk cell. This includes secretion of patterning signals and secretion of enzymes that process the nascent ECM. Furthermore, the rapid rearrangement of the cytoskeleton is likely to change the physical resistance the yolk cell can provide to support the morphogenesis of the overlying embryo.

Disruption of these features of yolk cell function will result in specific phenotypes depending on the time of YSL disruption. I hypothesize that the contraction of the yolk cell is the primary defect in *pwg* mutants, and the effect on the overlying germ layer morphogenesis is the result of loss of a set of YSL functions.

### **3.6 *mxtx1* genetically interacts with *pwg* to regulate yolk integrity**

A phenotype similar to that of *pwg* is produced by morpholino knockdown of *mixed-type homeobox1 (mxtx1)* in *natter/fibronectin1*



heterozygotes (Sakaguchi et al., 2006). Since *mxtx1* is expressed in the YSL and regulates *fibronectin1*, I investigated the relationship of *mxtx1* and *fibronectin1* with *pwg*. I injected embryos from *pwg* mutant females with 2 ng of a translation-blocking *mxtx1* morpholino (*mxtx1-mo*; Sakaguchi et al., 2006) into the YSL at 3 hpf and observed an increase in the *pwg* phenotype penetrance at 24 hpf (Fig. 3.6A; n=199, p-value < 0.001). These data indicate that both *mxtx1* and *pwg* act together to regulate YSL cytoskeletal integrity.

I tested whether the interaction of *mxtx1* with *fn1* (Sakaguchi et al., 2006) produced embryos with similar YSL catastrophe. I found that coinjection of *fn1-mo* (at 1-cell stage) and *mxtx1-mo* (into the YSL) into wild type embryos was able to recapitulate the yolk cell collapse phenotype similar to that observed in *pwg* mutant embryos (Fig. 3.5C). This result supports our observation that YSL collapse is associated with the *pwg* morphogenetic defects by 24 hpf. However, while injection of 4 ng of a translation-blocking *fibronectin1* morpholino into 1-cell *pwg* clutches was sufficient to delay cardiac precursor migration at 18 hpf in non-*pwg* embryos (Fig 3.6; (Trinh and Stainier, 2004), it did not increase the penetrance of the *pwg* phenotype in these embryos (Fig. 3.5B). This was unexpected, because Mxtx1 activity in the yolk has previously been shown to non-autonomously regulate expression and secretion of Fibronectin1 monomers from the blastoderm (Arrington and Yost, 2009; Sakaguchi et al., 2006). Taken together, our data show that *pwg* acts with *mxtx1* but does not display a genetic interaction with *fn1*.

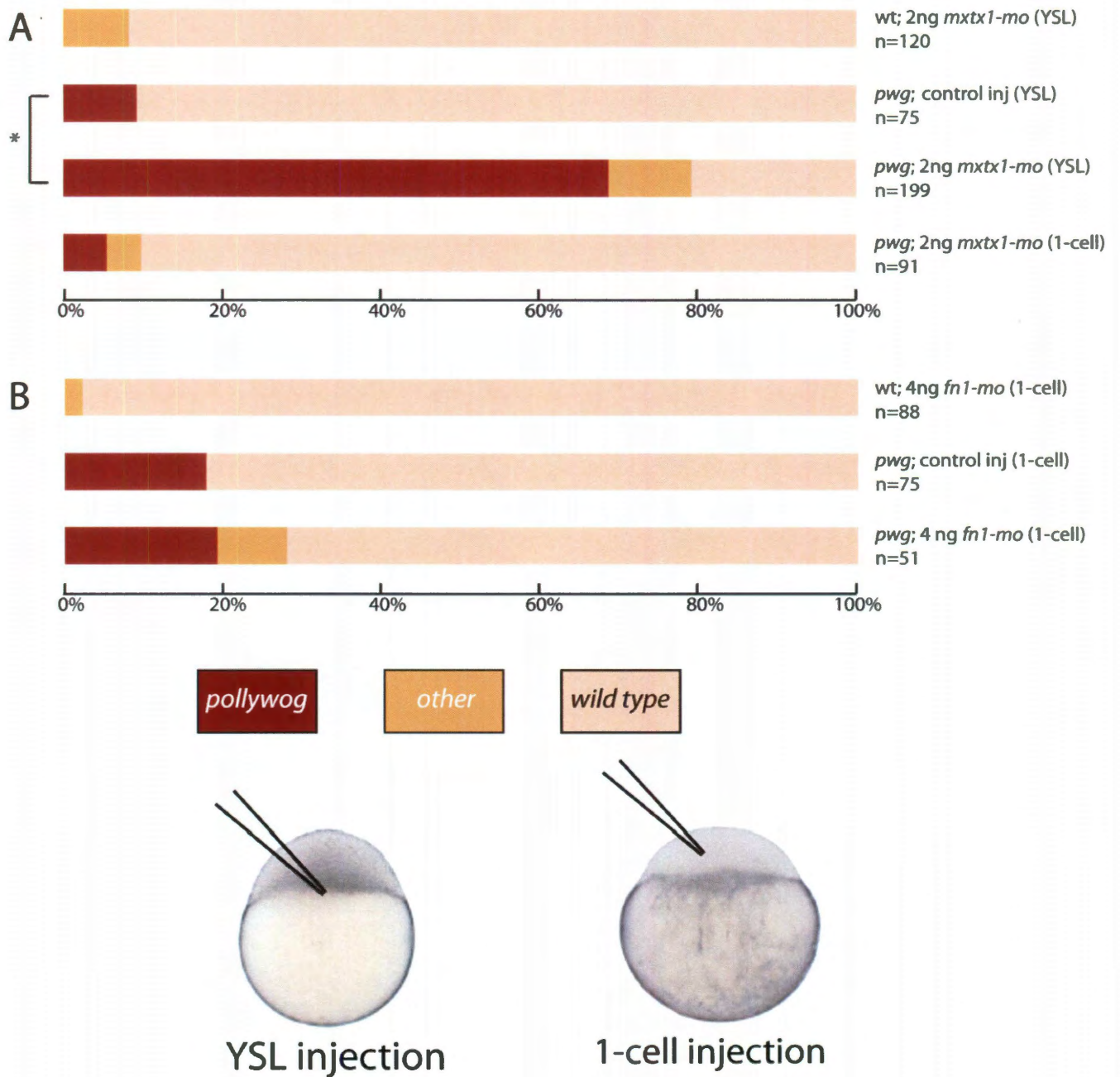


**Figure 3.6** (Legend on following page.)

**Figure 3.6** (Previous page) *mxtx1* genetically interacts with *pwg* but *fn1* does not. A: phenotype distribution of wild type or *pwg* embryos injected with *mxtx1*-mo. B: phenotype distribution of wild type or *pwg* embryos injected with *fn1*-mo. Significance (\* =  $p < 0.05$ ) is indicated by brackets and illustrations on right indicate location and stage of experimental microinjections.

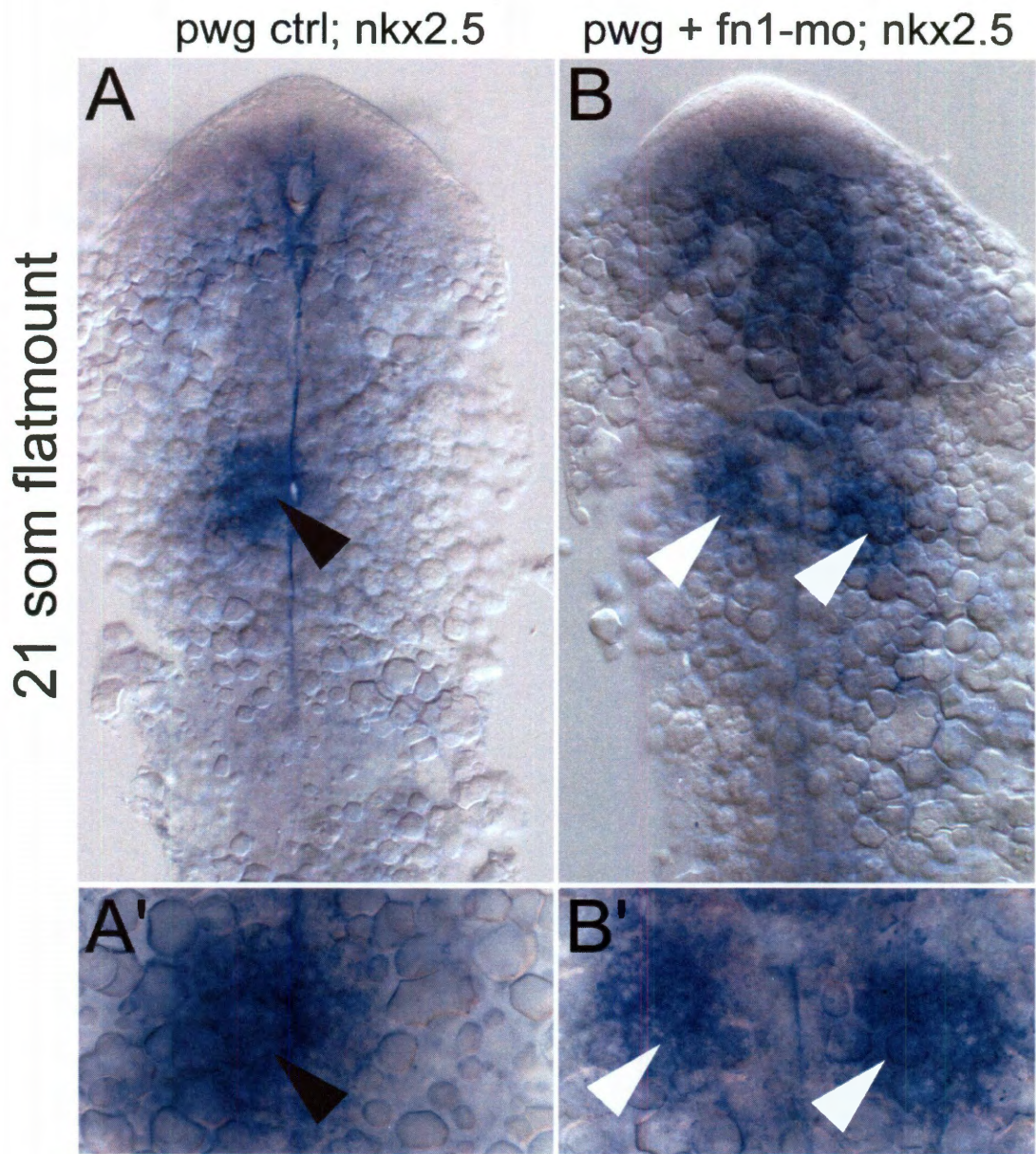


Figure 3.7 (Legend on following page)

**Figure 3.7** (Previous page) Injection of 4ng of *fn1*-mo into *pwg* mutant embryos causes cardia bifida but does not increase the penetrance of the *pwg* phenotype relative to control-injected siblings. A and B: flatmount views of *pwg* embryos at 21 somites stained for *nkx2.5* expression following control injection (A) or *fn1*-mo (B). A' and B': Close up views of the cardiac precursors. In control *pwg* embryos, the cardiac precursors have migrated medially to form the heart tube (black arrowheads in A and A') while in *fn1*-mo injected *pwg* embryos the cardiac precursor cells are still separated (white arrowheads in B and B').

### 3.7 *pwg* encodes zebrafish *map3k4*

*pwg* was mapped by meiotic recombination within a critical interval of 2.8cm on chromosome 13 that contained over 60 genes (Fig. 3.8A). *mxtx1* is on chromosome 13 but lay outside of our critical interval, eliminating it as a potential candidate. Because dominant negative *p38a* MAPK RNA injections phenocopy *pwg* (Fig. 3.4), I examined candidates within our critical interval for candidate genes that had known roles in MAPK signaling and found three such candidates: *Mediator of Cell Motility-1 (memo1)*, *mitogen-activated protein kinase kinase kinase kinase 5 (map4k5)* and *mitogen-activated protein kinase kinase kinase 4 (map3k4)*. I sequenced all three genes and identified a lesion in the *map3k4* open reading frame that results in an aspartic acid to tyrosine amino acid change at position 1044, which lies in a conserved region required for homodimerization of Map3k4 (Fig 3.8B; (Mita et al., 2002; Miyake et al., 2007). This nucleotide change was not present in the originally mutagenized male (data not shown; (Dosch et al., 2004; Wagner et al., 2004) and the altered amino acid is conserved in mouse and human MAP3K4 (Fig 3.8B).

In mammals, MAP3K4 functions as an upstream activator of the p38 MAPK module (Craig et al., 2008; Takekawa et al., 1997). Loss of Map3k4 or its kinase activity results in neural tube defects (Abell et al., 2005; Chi et al., 2005). Prior to activation, MAP3K4 exists as an auto-inhibited monomer. Upon activation by GADD45, the N-terminal autoinhibitory domain

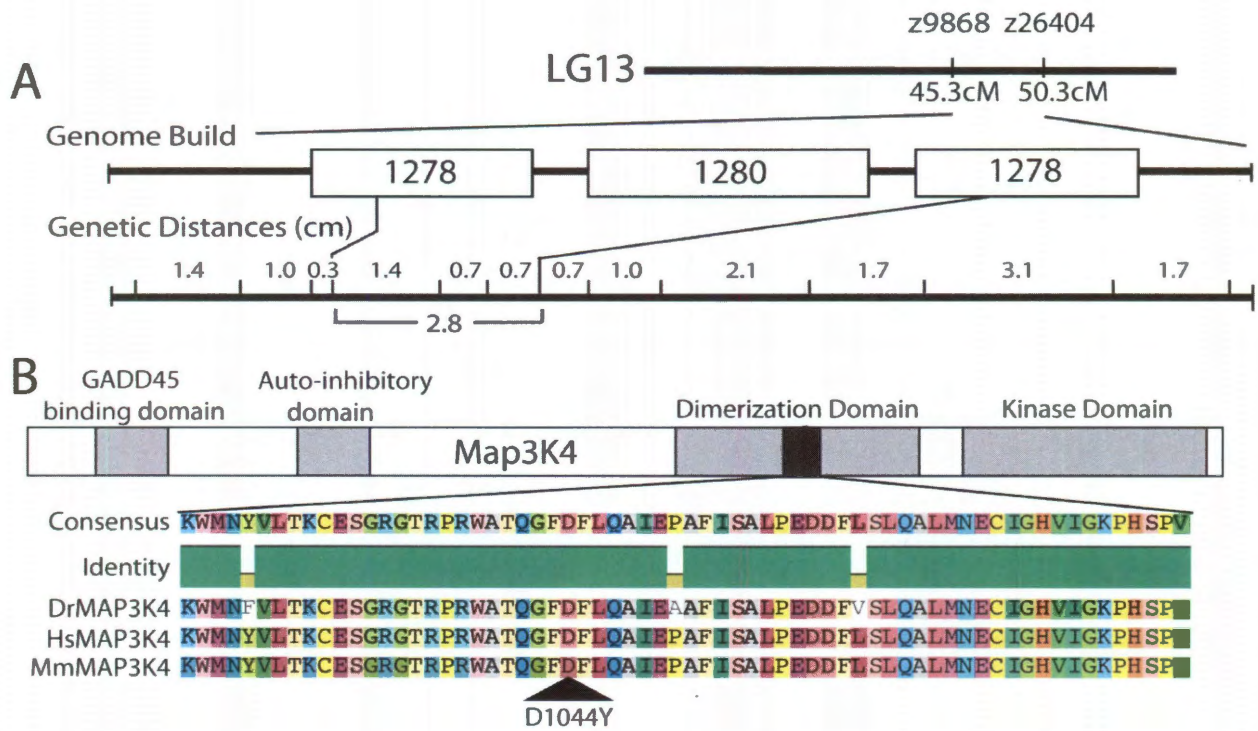


**Figure 3.8 A-B.** *pwg* encodes the zebrafish *map3k4*. A: the *pwg* critical interval on chromosome 13. B: diagram of the described domains of human MAP3K4.

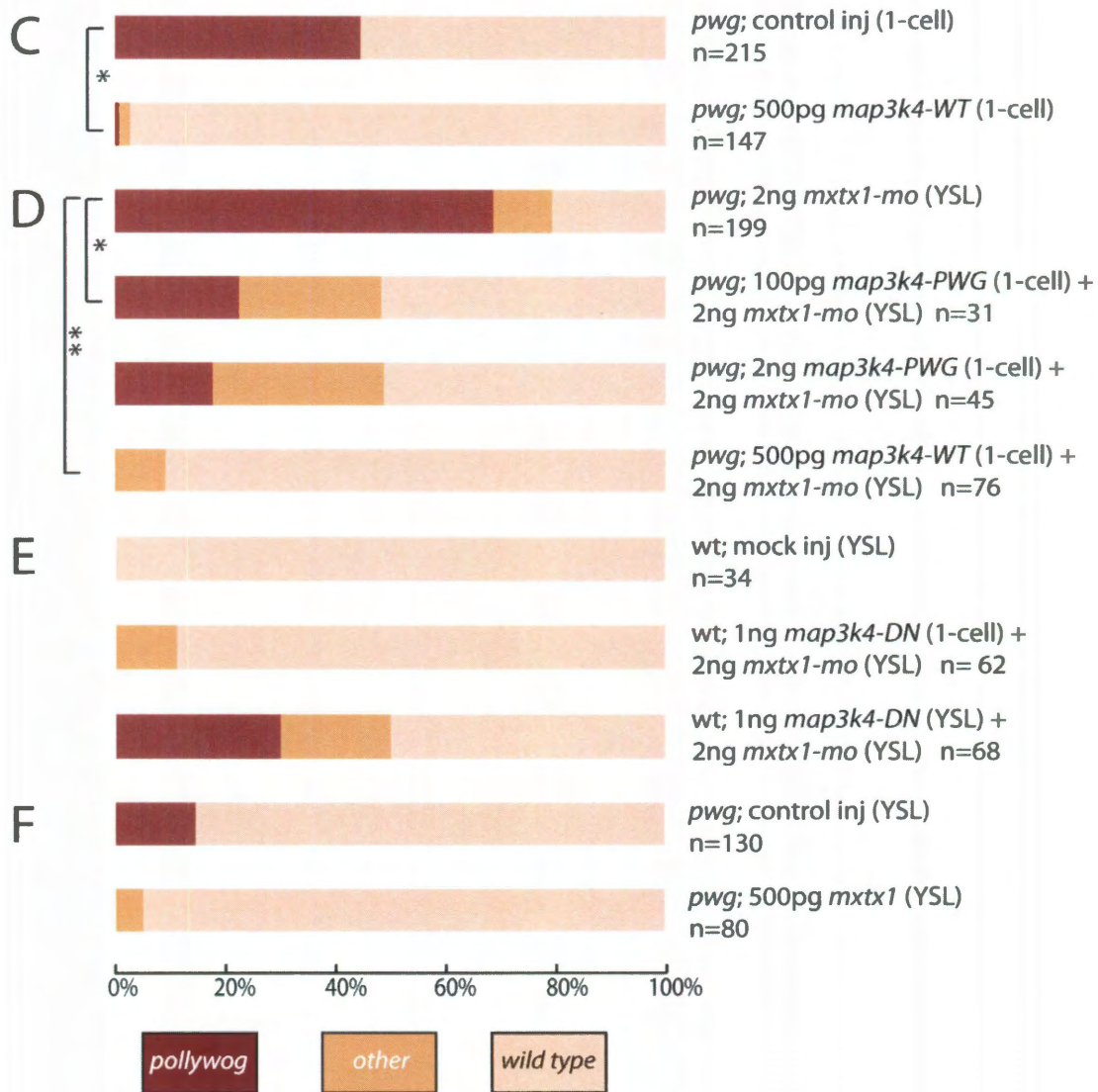


**Figure 3.8 C-F.** *pwg* encodes the zebrafish *map3k4*. C-F: phenotype distribution following injection of the indicated solutions. Significance is indicated by brackets (\* =  $p < 0.05$ , \*\* =  $p < 0.005$ ).



dissociates from the dimerization domain, allowing homodimerization and trans-phosphorylation (Mita et al., 2002; Miyake et al., 2007; Takekawa and Saito, 1998; Takekawa et al., 2002). This activated MAP3K4 complex is then localized to the nuclear periplasm where it activates downstream MAP2Ks (Craig et al., 2008). The missense mutation in the dimerization domain is likely to disrupt activation of Map3k4.

To directly test *map3k4* as the identity of *pwg*, I injected *pwg* embryos with RNA encoding the wild type *map3k4* gene (*map3k4-WT*). I observed that injection of 500 pg of *map3k4-WT* RNA successfully rescues *pwg* mutant embryos (Fig. 3.8C; n=147, P<0.001). Expression of as much as 2 ng of *map3k4-WT* RNA in wild type embryos resulted in no obvious morphogenetic defects (data not shown).

I tested the activity of *pwg* mutant *map3k4* RNA (*map3k4-PWG*) in *mxtx1-MO* injected embryos. I found that injection of 100 pg of *map3k4-PWG* RNA bearing the D1044Y mutant allele could decrease the penetrance of the *pwg* phenotype in mutant clutches injected with *mxtx1-mo* (Fig. 3.8D; n=31, p<0.001), while a 10-fold higher dosage (1 ng) of *map3k4-PWG* RNA still did not rescue the same number of *pwg* mutant embryos as supplying 500 pg wild type transcript (Fig. 3.8D; n=76, P<0.0001). These data indicated that *pwg* is a hypomorphic allele of *map3k4* with reduced function. Interestingly, injection of *map3k4-WT* RNA rescued these *pwg* clutches as efficiently with or without knockdown of *mxtx1* (compare Fig. 3.8C and D).

To confirm the identity of *pwg* as *map3k4* I blocked Map3k4 activity by injection of RNA encoding a kinase-dead dominant negative *map3k4* construct (Takekawa and Saito, 1998; Takekawa et al., 1997). These were unable to phenocopy *pwg* when injected into 1-cell stage wild type embryos or into the YSL (data not shown). I suspected that, as in the case of *pwg* mutants, *mxtx1* knock-down could potentiate an effect of dominant negative *map3k4* and *map3k4* morpholinos to phenocopy *pwg*. I tested if coinjection of these reagents along with *mxtx1* morpholino would phenocopy *pwg*. Following co-injection of 1 ng of *map3k4-DN* RNA and 2 ng *mxtx1-mo* into the YSL of wild type embryos, I observed phenocopy of *pwg* (20 out of 68 embryos, Fig 3.8E). Similar experiments using a *map3k4* translation-blocking morpholino were less efficient, likely due to maternal Map3k4 protein in wild type embryos (data not shown). The fact that microinjection of these reagents into the YSL was sufficient to phenocopy *pwg* indicates that Map3k4 activity is required in the YSL for proper yolk cell morphogenesis and acts non-autonomously to influence morphogenetic movements in the overlying blastoderm.

Since *mxtx1* and *pwg* display a genetic interaction, I examined the ability of *mxtx1* RNA to rescue *pwg* mutants. I hypothesized that if *mxtx1* has a role either upstream or downstream in the same processes as *map3k4* to coordinate yolk morphogenesis via maintenance of YSL integrity, overexpression of *mxtx1* RNA would rescue the hypomorphic *pwg* allele. However, if they act in different pathways, I would not observe such a rescue.

I observed that injection of 500 pg of *mxtx1* RNA in the YSL was sufficient to rescue the *pwg* phenotype at 24 hpf (Fig. 3.8F). Although these data do not establish a specific epistatic relationship, they indicate that both *mxtx1* and *map3k4* are involved in YSL stability.

The most direct explanation for the *mxtx1-pwg* interaction is that *pwg* is a maternal factor required for the yolk specific expression of *mxtx1*, as proposed by Sakaguchi et al. I examined the expression of *mxtx1* during early and late gastrulation in *pwg* mutants by whole mount in situ hybridization in a clutch with 8% penetrance (n=50 siblings scored at 24 hpf). No loss of YSL *mxtx1* expression was observed at 60% epiboly (n=32) or at 100% epiboly (Fig. 3.9, n=69), indicating *pwg* is unlikely to act upstream of *mxtx1* expression.

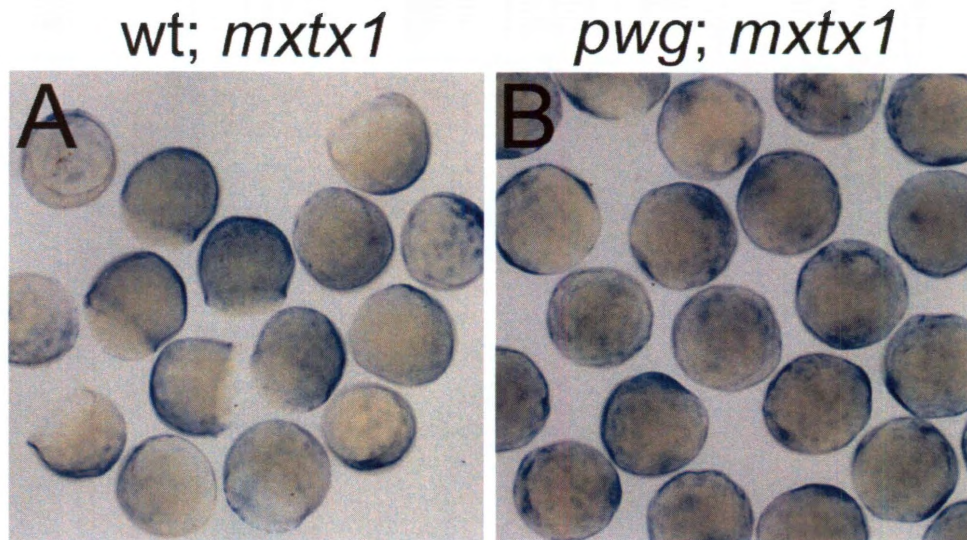


**Figure 3.9.** *mxtx1* expression is retained in *pwg* mutant embryos. A and B: low magnification image showing a mix of expression of *mxtx1* in the YSL at stages from shield to 90% epiboly in wild type (A) and *pwg* mutant (B) embryos.

### 3.8 *gadd45 beta b*, a possible upstream activator of *map3k4*

In order to examine a possible requirement for GADD45-mediated activation of Map3k4, I injected 20ng of *gadd45-mo* into wild-type embryos to see if it could phenocopy *pwg*. I observed that morpholino-mediated knockdown of *gadd45beta-b*, but not *gadd45beta-a* (data not shown), could recapitulate both the early prechordal plate phenotype at very high concentrations of injected morpholino (20 ng), but only in a very small number of embryos (n=7 *pwg* phenocopies, n=112 unaffected embryos). In affected *gadd45bb* morphants, expression of *hgg1* shows that the prechordal plate fails to migrate beyond the overlying neural/non-neural boundary by bud stage (Fig. 3.10B), as well as plunges into the yolk (Fig. 3.10E). At 24 hpf, affected embryos have a flattened head, visible disruption of the yolk and tail extension defects similar to those observed in *pwg* mutants (data not shown).

Because of non-specific morpholino toxicity, co-injection with *p53-mo* was performed in all experiments to reduce the apoptotic response following completion of gastrulation in response to this toxicity effect. Although *p53-mo* was able to reduce the toxic effect, it was unable to completely eliminate it, thus making the apparent phenocopy of *pwg* difficult to interpret, since it could be part of the toxicity response in these embryos.

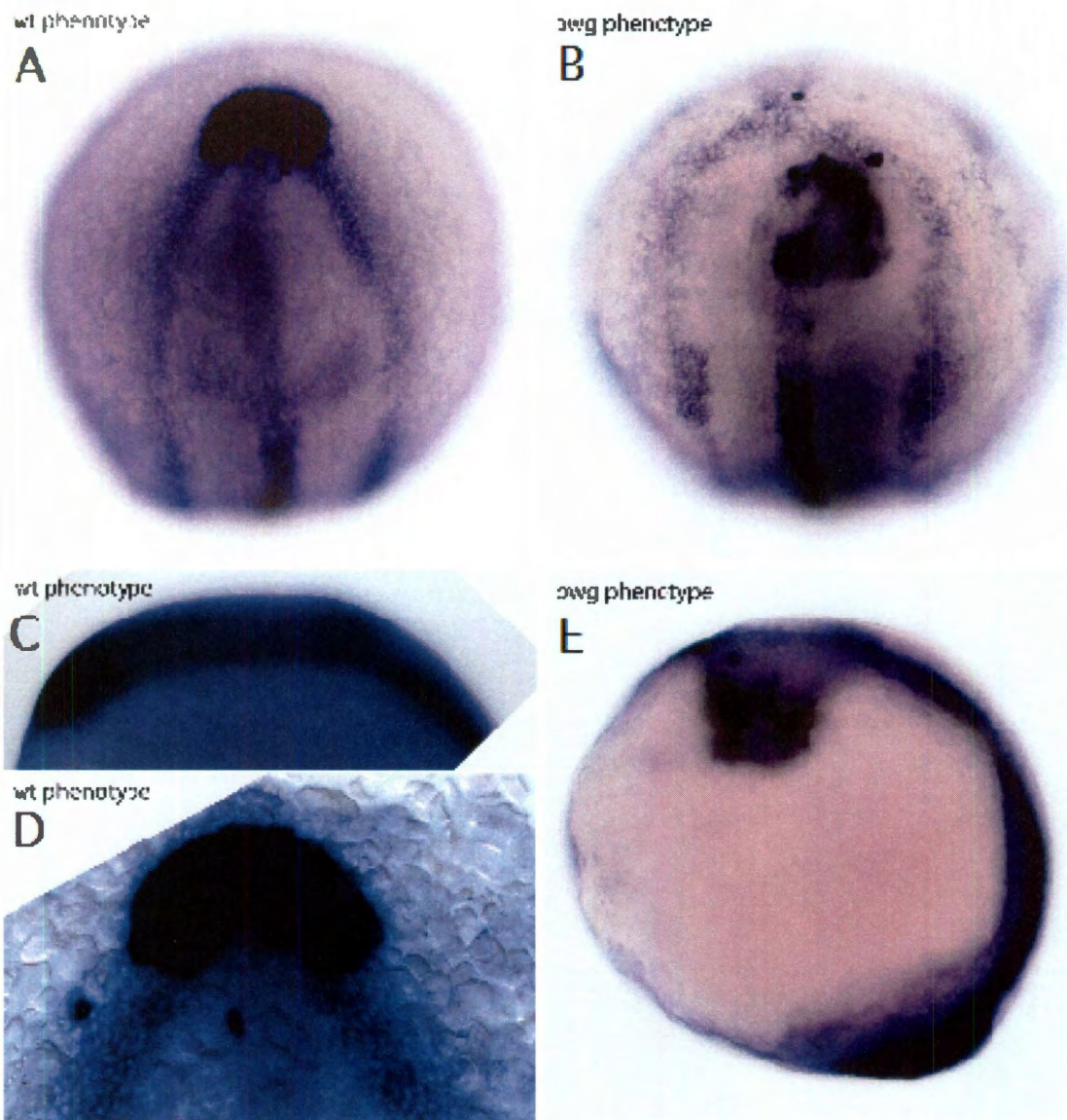


**Figure 3.10.** Morpholino knockdown of *gadd45 beta b* possibly recapitulates the *pwg* phenotype. A-E: *in situ* hybridization assays of *hgg1*, *pax2.1*, *shh* and *dlx3*. A, C and D are morphant embryos that appear wild type in morphology (compare to Fig. 3.2). A and D animal views, C is a lateral view). B and E are animal are *pwg* phenotype-bearing *gadd45 beta b* morphants shown in animal and lateral views, respectively.

## **Chapter 4: The alpha-actinin gene family**

### **4.1 Brief statement from the author**

My work with zebrafish alpha-actinins stems from an early observation made while evaluating *alpha-actinin1/actn1* as a candidate for *pwg*. RT-PCR performed using primers designed to amplify the 3' region of *actn1* failed to produce an amplicon when using *pwg* ovary-derived cDNA template in these reactions. Subsequently, 3'- and 5'-RACE and Northern blotting failed to produce any concrete data in *pwg* mutants. However exhaustive sequencing of *actn1* 3'UTR, 5'UTR, open reading frame, as well as all 22 splice donor and splice acceptor sites for *actn1* in *pwg* mutants eventually revealed no significant nucleotide change that could indicate that *pwg* encoded *actn1*. I decided to use the extensive alpha-actinin data that we had to do a survey of alpha-actinins and their expression during development. This work was published in *Developmental Dynamics* and I received assistance from other authors on the publication (Holterhoff et al., 2009).

### **4.2 Introduction**

Actinins are a family of actin-binding proteins that have diverse functions (Beggs et al., 1992). Despite the radical spectrum of actinin function, most members of the actinin family are highly conserved, suggesting very strict evolutionary constraints act upon these genes (Chan et al., 1998). All model tetrapods have four actinin family members except avian genomes, which have three. All members possess an N-terminal actin-binding domain

(ABD) followed by four  $\alpha$ -helical spectrin-like repeats and a C-terminal calmodulin (CaM) domain with two EF-hand motifs. Actinins function as anti-parallel dimers, resulting in a flexible, rod-like structure able to bind f-actin at each of its two N-terminal heads (Burrige and Feramisco, 1981). Actinins 1 and 4 are referred to as cytoplasmic or non-muscle actinins. They bind to actin filaments throughout the cytoplasm and have been shown to decrease their affinity to actin stress fibers and focal adhesion scaffolds upon calcium treatment (Otey and Carpen, 2004). In addition to binding actin via their ABD, actinins 1 and 4 directly bind a multitude of other proteins along their spectrin repeats, presumably regulating their localization or function (Weins et al., 2007).

In mice, *Actn4* is required for maintaining podocyte function in the kidney glomerulus (Michaud et al., 2009). Supporting a role regulating the actin cytoskeleton architecture, *Actn4* knockouts display disorganization of podocyte microfilaments in response to changes in hydrostatic pressure (Kaplan et al., 2000; Weins et al., 2007). In humans, dominant negative alleles of *ACTN4* are associated with Focal and Segmental Glomerulosclerosis (FSGS; OMIM:603278) due to uncoupling of  $\text{Ca}^{+2}$ -binding from microfilament release by ACTN4, resulting in unresponsive and actin-bound populations of ACTN4 (Geeves and Holmes, 1999).

Actinins 2 and 3 are highly expressed in muscle fibers, where they function to maintain microfilament spacing at the Z-disc (Beggs et al., 1992; Geeves and Holmes, 1999). The muscle-specific actinins have different



activities than the non-muscle actinins. While they bind actin microfilaments, they are unable to bind calcium with their CaM domain EF-hands and are largely restricted to the Z-discs of striated muscle and analogous actin-rich dense bodies (Costa et al., 2002). Muscle-specific actinins are expressed during the earliest stages of myofibril formation in the zebrafish (Costa et al., 2003; Sanger et al., 2009). The zebrafish actinins localize to the Z-disc early in myofibrillogenesis (Chowrashi et al., 2002; Frey and Olson, 2002). Expression of particular muscle-specific actinins correlates with differences in muscle physiology. Muscle actinins have been shown to bind to amorphin and members of the calsarcin family and localize them to the Z-disk (Serrano et al., 2001). These proteins may in turn associate with calcineurin to regulate differentiation of myofiber types (Mills et al., 2001; North and Beggs, 1996). *ACTN2* and *ACTN3* may interact with different complements of proteins to regulate muscle physiology. In adult human muscle, *ACTN2* is present in all skeletal muscle, while *ACTN3* is active in only a subset of type II (fast) muscle fibers (Mills et al., 2001). In mouse skeletal muscle, there is an incomplete overlap in *Actn2* and *Actn3* expression, leaving some muscle fibers expressing only *Actn3* (Chan et al., 1998). There is also evidence that human *ACTN2* and *ACTN3* molecules can form heterodimers *in vitro* and *in vivo*, indicating potential additional physiological complexity resulting from overlapping expression (North et al., 1999). A null allele of *ACTN3* containing a premature stop codon at Arginine 577 is estimated to be homozygous in 16% of the human population (Yang et al., 2003). Further analysis revealed a

significant positive selection for *ACTN3*<sup>R577X</sup> homozygotes among female endurance athletes, indicating that loss of ACTN3 promotes an efficient muscle phenotype (Yang et al., 2003). There is also a negative correlation for *ACTN3* mutation in elite sprinter athletes who have predominately fast twitch muscle (MacArthur et al., 2007). This concordance with performance in humans suggests that the presence or absence of the full-length ACTN3 protein significantly impacts muscle physiology and performance. Supporting this hypothesis, mice lacking ACTN3 activity show a shift to aerobic metabolism, resulting in efficient muscle function and increased endurance (Beggs et al., 1992; MacArthur et al., 2007).

Taken together, the above observations indicate diverse functional roles for this highly related gene family. We chose to examine the temporal and spatial regulation of zebrafish actinins as a first step in understanding the functional requirements of actinins in teleost development. We identified clear zebrafish homologs of all tetrapod actinins including two of the three splice isoforms of human *ACTN1* as well as two orthologs of human *ACTN3*. We found that the non-muscle *actn1* is widely expressed. *actn4* displays higher expression in the notocord. We observed expression of *actn2*, *3a* and *3b* in overlapping sets of muscle, implying a contribution of these genes to physiological specialization of muscles. In particular *actn2* is highly expressed in cardiac muscle and a subset of slow twitch skeletal muscle while *actn3a* and *actn3b* are highly expressed in the axial muscles and have differential expression in cranial and pharyngeal muscles. The diverse

expression patterns of the actinins indicate substantial specialization of individual genes within this highly related gene family. The duplication of *actn3* and divergent expression of both paralogs in the zebrafish contrasts with its positive selection for a non-functioning allele in human populations and absence in chicken. These observations indicate that diversification of *actn3* expression or activity may be an effective mechanism for regulating muscle physiology in response to selective pressure.

### **4.3 Identification of zebrafish alpha-actinin homologs**

Zebrafish alpha-actinin family members were initially identified by reciprocal BLAST searches using annotated human actinins to identify homologs in the zebrafish genome (see Experimental Procedures). We were able to identify five unique zebrafish actinin genes, located on linkage groups 7, 13, 17 and 21 as well as another actinin that has not yet currently been placed on any of the 24 zebrafish chromosomes as of the release of genome build Zv8 (Sanger Center). The zebrafish actinins sorted into existing phylogenetic clades when aligned with other vertebrate family members (Fig. 4.1A). The *actn3* clade revealed the presence of two distinct zebrafish *actn3* members (Fig. 4.1A). In light of the apparent dispensability of ACTN3 in humans and mice (Burrige and Feramisco, 1981; Haiech et al., 1991) the presence of two active and conserved *actn3* genes in zebrafish may represent differences in muscle physiology and adaptation among vertebrates. These two zebrafish Actn3 proteins show a striking sequence

divergence with only 92.9% identity. This falls within the range of percent identity conserved between the zebrafish genes and their human homologs, with these pairs showing at least 82.5% identity (*actn3a::ACTN3*) and at most sharing 93.4% identity (*actn1 iso b::ACTN1 iso b*) at the amino acid level (Fig. 4.1B). The assignment of gene identity was confirmed by analysis of syntenic conservation between human and zebrafish actinin gene regions. Each homolog had clear local conservation of homologous genes in the corresponding genome including the duplicated *actn3* genes. No additional actinin genes were identified by searches of EST or genomic databases, therefore we expect that these five actinins represent the full complement of zebrafish actinin genes.

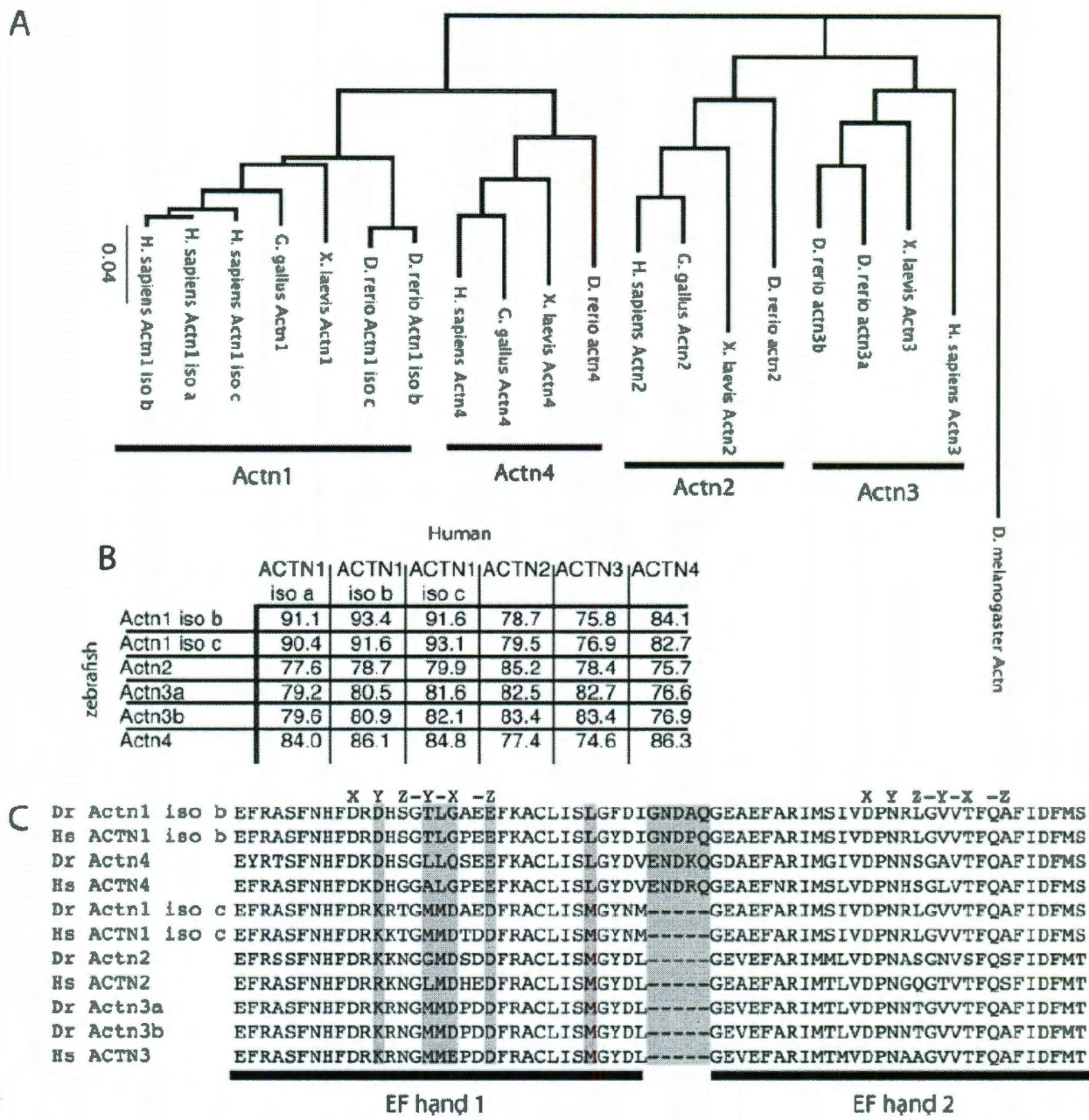


Figure 4.1. (Legend on following page).

**Figure 4.1.** (From previous page.) The zebrafish genome contains five actinin genes representing the four major classes of mammalian actinins. A: Jukes-Cantor nearest neighbor tree of zebrafish, tetrapod and *Drosophila* actinins. B: Percent identity of Human and zebrafish actinins. C: Alignment of EF hands 1 and 2 of Human and zebrafish actinins. Coordinating residues X, y, Z, -Y, -Z are indicated. Positions with conservation of Actn1 iso C with the muscle-specific actinins are highlighted in grey.

Calcium binding is a feature of CaM domain EF-hands (Arimura et al., 1988; Beggs et al., 1992; Burridge and Feramisco, 1981; Janssen et al., 1996; Tang et al., 2001; Witke et al., 1993), and previous work has shown that microfilament binding of non-muscle actinins can be regulated by intracellular  $\text{Ca}^{2+}$  levels while muscle-specific actinin activity is not (Beggs et al., 1992; Tang et al., 2001). We aligned the first 2 EF-hands of human and zebrafish actinins to determine their conservation. We observed that both EF-hands found in Actn3a and 3b were 100% identical and differ from the human ACTN3 at 4 of 63 amino acids (Fig. 4.1C). The Actn2 EF hands were more divergent with changes in 12 of 63 amino acids. Actn2, Actn3a and Actn3b all have substitutions at the critical Y position in EF hand 1 that is essential for  $\text{Ca}^{2+}$  binding, indicating that like mammalian muscle actinins they are not regulated by calcium (Devoto et al., 1996). We identified two splice isoforms of *actn1* both of which are homologous to isoforms identified in humans. These isoforms utilize alternate exons within the EF hand domains (Fig. 4.1C). The c isoforms of both human and zebrafish have substitutions at positions essential for  $\text{Ca}^{2+}$  binding and lack 5 amino acids between the EF hands, indicating these isoforms are likely similar to the muscle actinins in their calcium binding activity. Actn1 isoform b and the Actn4 protein contain all of the essential amino acids for calcium binding.

#### 4.4 Temporal expression profile of zebrafish alpha-actinin genes

If the actinins have specific functions during development of the zebrafish embryo we would expect the expression to vary during development of the embryo. We performed RT-PCR reactions to determine the temporal profile of each actinin (Fig. 4.2). We tested a broad range of time points beginning with maternal ovary and developing oocytes through 8 days post fertilization (dpf) larval stage cDNA samples. To determine the level of expression, we performed RT-PCR reactions with 25, 30 or 35 rounds of amplification for each actinin to obtain at least one sample within a linear amplification range. All primer pairs spanned at least one intron to distinguish between cDNA and genomic DNA amplification. Transcripts for the cytoplasmic actinins *actn1* and *actn4* are present maternally and persist throughout embryogenesis, with *actn4* appearing to be more abundant in whole-embryo cDNA samples. The muscle actinins were expressed at low levels maternally. *actn3b* expression persisted at low levels through gastrulation. All muscle actinins were robustly expressed by 24 hours post fertilization (hpf) and continued to be expressed through the time course.



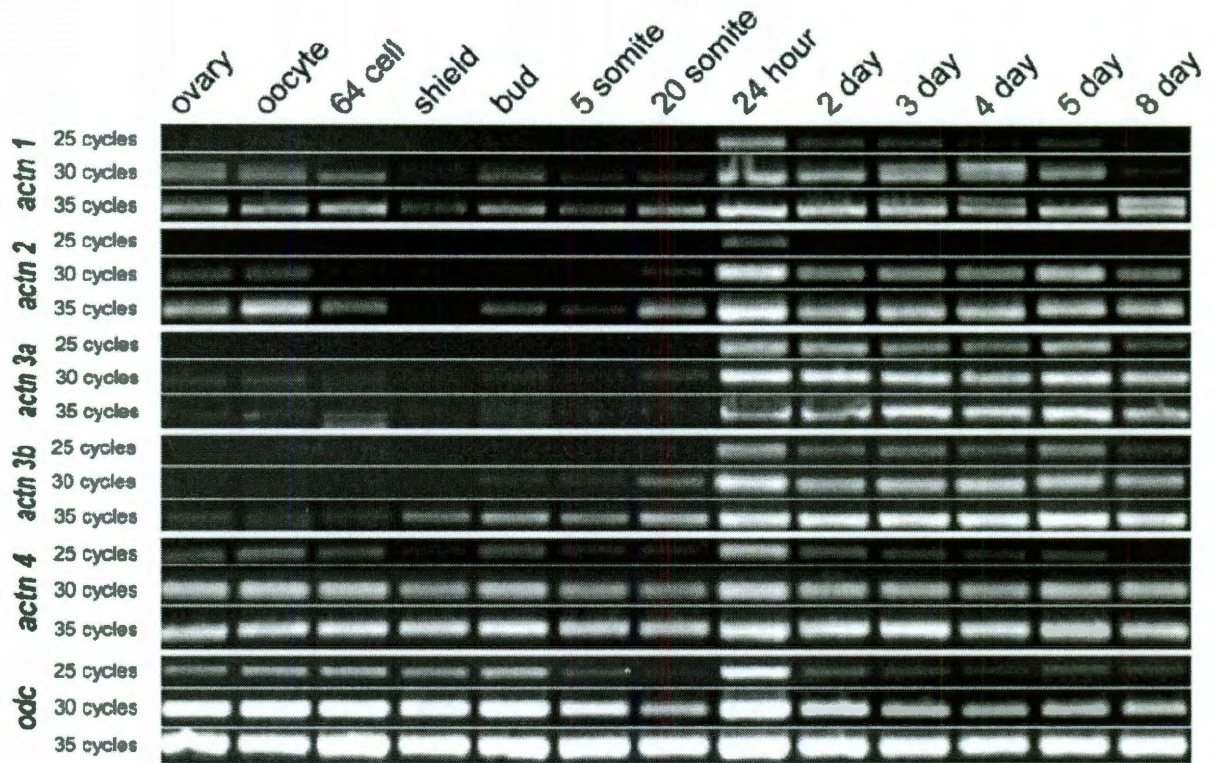


**Figure 4.2.** Temporal expression profiles of zebrafish actinin genes as shown by semi-quantitative PCR. Each actinin gene shows a unique and dynamic regulation of expression through early development. cDNA samples used for each PCR reaction are indicated by column and range from adult ovary and oocytes to 8 dpf larval cDNA. The upper band of the *actn1* doublet was sequenced to show it is a product from an unrelated locus.

#### **4.5 Tissue specific expression of zebrafish actinins**

We performed *in situ* hybridization reactions in order to visualize which tissues expressed each actinin during development. We included an early time point (64-cell stage) prior to initialization of zygotic transcription to observe maternal message as well as stages associated with the beginning of gastrulation (shield stage), blastopore closure (bud stage), onset of segmentation and somitogenesis (5- and 10-somite stages) as well as later larval stages during myogenesis in the maturing somite mesoderm, pharyngeal arches and cranium (24, 36, 48 and 96 hpf).

#### **4.6 *actn1* and *actn4*: the non-muscle actinins**

*actn1* and *actn4* mRNAs were ubiquitously expressed at maternal stages through segmentation (data not shown). However at 36 hpf, enrichment of *actn1* was observed in the notochord and skin (Fig. 4.3F) in transverse sections. *actn1* was also expressed throughout the 36 hpf somite but was markedly absent from the central nervous system (Fig. 4.3F').

At 36 hpf, *actn4* was not widely expressed. *actn4* was highly expressed in the notochord and the developing gut, but was excluded from neural tissues at these larval stages (Fig. 4.3G&G')

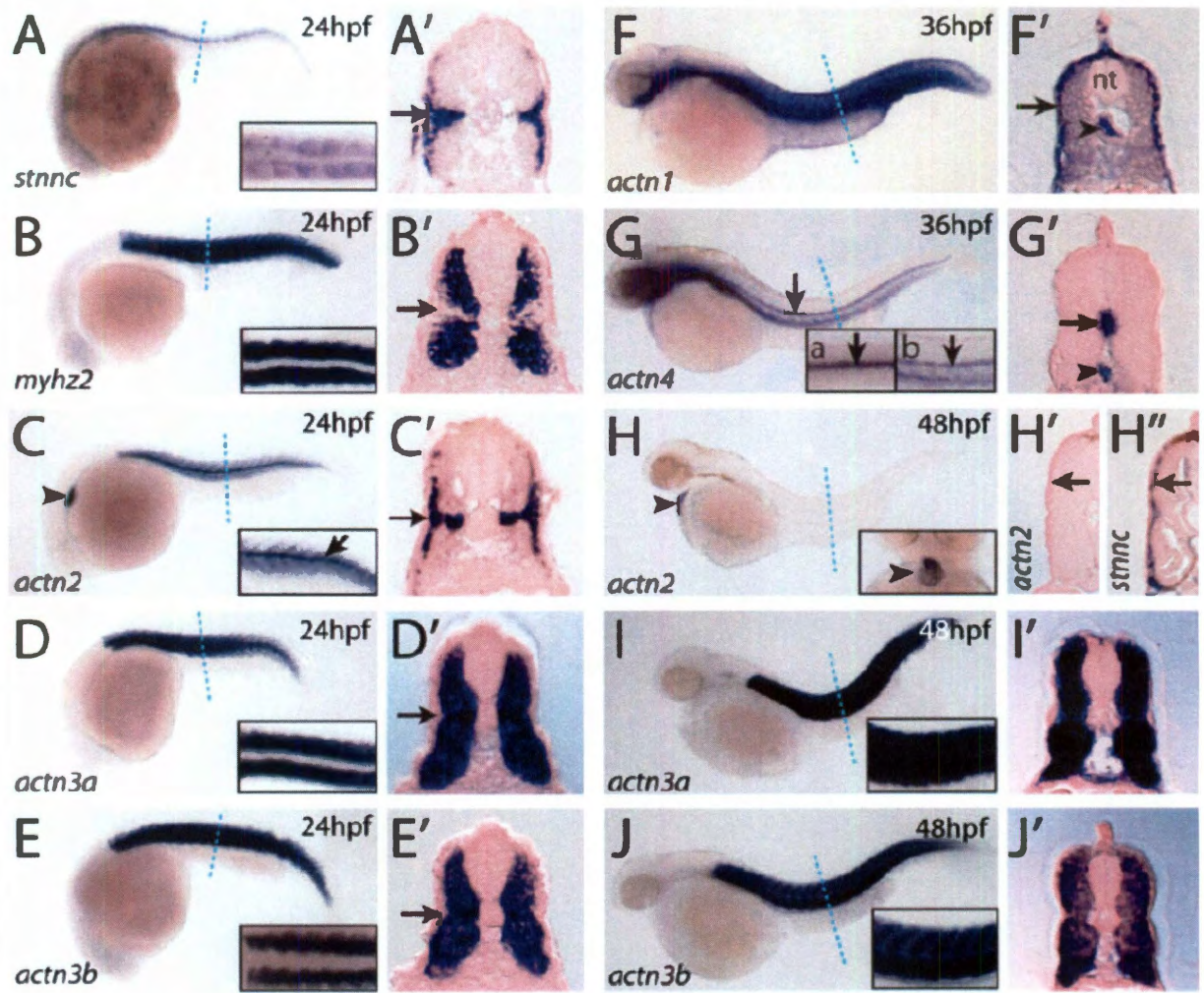


**Figure 4.3.** (Legend on following pages.)

**Figure 4.3.** Expression of the actinin gene family at 24-48 hpf. Expression of the actinins by whole mount in situ hybridization reveals distinct patterns for most genes. A-J: lateral whole mount views with insets showing higher magnification dorsal or lateral views of somite gene expression, insets are magnified lateral (C,Gb,I,J), dorsal (A,B,D,E,Ga) or anteroventral (H) views); A'-J': transverse sections of axial gene expression taken at level indicated by blue lines in A-J. A,A': Expression of slow-specific marker *stnnc* at 24 hpf. Expression was observed in slow muscle fibers including muscle pioneer cells (arrow) and in peripheral slow muscle sheath. B,B': Expression of fast-specific marker *myhz2* at 24 hpf. Expression is seen in most of the somite but no expression is seen in the muscle pioneer cells (arrow). C,C': Expression of *actn2* at 24 hpf. Expression is seen in the heart (arrowhead) and in the slow muscle pioneers (arrows). D,D',E,E': Expression of *actn3a* (D,D') and *actn3b* (E,E') at 24 hpf. Both *actn3a* and *actn3b* are widely expressed in the somite. Expression is also seen in the slow muscle pioneer cells (arrows). F,F': Expression of *actn1* at 36 hpf. Expression was observed in the skin (arrow), notochord (arrowhead) and generally expressed in the somite. Expression was not observed in the neural tube (nt) or other components of the CNS. G,G': Expression of *actn4* at 36 hpf. Expression is seen in the notochord (arrows) as well as the developing gut (arrowhead). H,H': Expression of *actn2* at 48 hpf. Expression is seen in the heart (arrowheads) but is no longer observed in the slow muscle fibers of the myotome (arrow). H'': Expression of *stnnc* at 48 hpf. Expression can be

**Figure 4.3 (continued)** seen in the peripheral sheath of slow muscle fibers (arrow). I,I',J,J': Expression of actn3a (I,I') and actn3b (J,J') at 48 hpf. Both actn3a and actn3b are broadly expressed in most or all of the myotome muscle fibers.

#### **4.7 *actn2, actn3a, actn3b*: the muscle actinins during axial muscle development**

In our RT-PCR analysis we detected maternal expression of all three muscle actinins. In whole mount *in situ* hybridization *actn2* was distributed ubiquitously at maternal stages and at shield stage (data not shown).

In contrast to mammalian limb muscle, the zebrafish axial muscle of the trunk and tail displays strict separation of slow and fast muscle into distinct spatial domains (Blagden et al., 1997; Devoto et al., 1996). Lineage tracing experiments have shown that slow (Type I) muscle fibers arise primarily from adaxial cells adjacent to the notochord (Devoto et al., 1996; Hollway and Currie, 2003). Subsequently, these cells migrate laterally and by 24 hpf, these cells have expanded dorsoventrally to create a sheet of slow muscle fibers extending along the lateral edge of the myotome (reviewed in Ochi and Westerfield, 2007). Fast (Type II) muscle fibers arise from the somite and compose the majority of the *myoD*-positive zebrafish myotome by 24 hpf (Elworthy et al., 2008). This spatial separation allowed us to examine fiber type specific restriction of expression of the muscle-specific actinins if it was present.

The first specific expression of *actn2* was at 15 somites with expression in the early differentiating adaxial cells immediately adjacent to the notochord. In transverse sections, expression of *actn2* was highest in these adaxial muscle progenitors. At 24 hpf, *actn2* was expressed in a mediolateral set of muscle fibers extending dorsoventrally along the lateral sides of the

somite (Fig. 4.3C&C'). This expression pattern is similar to the location of slow muscle cells. In order to determine if the muscle-specific actinins had expression patterns synonymous with slow or fast fiber types by 24 hpf, we performed RNA *in situ* hybridization with genes known to be restricted to slow or fast fibers in the zebrafish myotome. *slow-specific troponin C (stnnc)* (Peng et al., 2002) is expressed in slow fibers (Fig. 4.3A&A'), while *myosin heavy polypeptide 2 (myhz2)* (Peng et al., 2002) is exclusively expressed in fast muscle fiber during this time (Fig. 4.3B&B'). *actn2* was expressed in the same pattern as *stnnc* and in an opposite pattern to *myhz2*. *actn2* is also strongly expressed in the heart at 24 hpf (Fig. 4.3C). Strikingly, by 36 hpf and continuing to 48 hpf, *actn2* is absent from the slow muscle of the myotome and is only expressed in the heart while *stnnc* continues to be expressed in the slow muscle (Fig. 4.3H,H'&H'' and data not shown).

*actn3a* and *actn3b* expression was first detected by *in situ* hybridization at 10 somites (14 hpf) by whole mount *in situ* hybridization (data not shown). This expression was restricted to adaxial cells, but began to expand laterally by 15 somites. By 24 hpf, both *actn3a* and *actn3b* were strongly expressed throughout the somites (Fig 4.3D,I,E&J). This expression appears broader than the expression of the fast muscle marker *myhz2* (Devoto et al., 1996; Elworthy et al., 2008) and may encompass the domain of the slow muscle marker *stnnc* and *actn2*. At 36 hpf and 48 hpf, strong gene expression of *actn3a* and *actn3b* is still observed and appeared to encompass the entirety of the somites (Fig 4.3I&J and data not shown).

Because we do not observe expression of *actn2* in axial musculature at 48 hpf, it is likely that *actn3a* or *actn3b* or both are expressed in all slow and fast fibers at this stage.

By 96 hpf, *actn2* was once again expressed in axial muscle (Fig 4.4A&A'). Unlike earlier expression, where the *actn2* expression pattern was similar to the antibody staining profile of Slow-Type MyHC and the expression pattern of *stnnc* in all of the slow fiber domains of the 24 hour myotome (Blagden et al., 1997; Fig. 4.3A), at 96 hpf, expression of *actn2* is restricted to a narrow row of slow muscle cells that make up the presumptive lateralis superficialis muscle, with no expression detected in the sheath of Type I (slow) muscle cells that reside in the lateral periphery of the myotome at this stage (Ono et al., 2006). *actn2* is also expressed in the inferior obliquus muscle along the ventrolateral edge of the myotome (Fig. 4.4A inset). There are similarities between *actn2* expression at this stage of development and expression of a MyHC gene *mMYH<sub>C1</sub>* that is restricted to the lateralis superficialis from three to seven dpf in the Medaka axial muscles (Hernandez et al., 2005; Schilling and Kimmel, 1997). This restriction of *actn2* to only a small set of muscle fibers in the 96 hpf myotome contrasted with the expression patterns of *actn3a* and *actn3b*, which were both expressed throughout the 96 hpf larval myotome (Figure 4.4A',B'&C'). Both *actn3a* (65%, n=17) and *actn3b* (65%, n=14) showed variable lateral, superficial



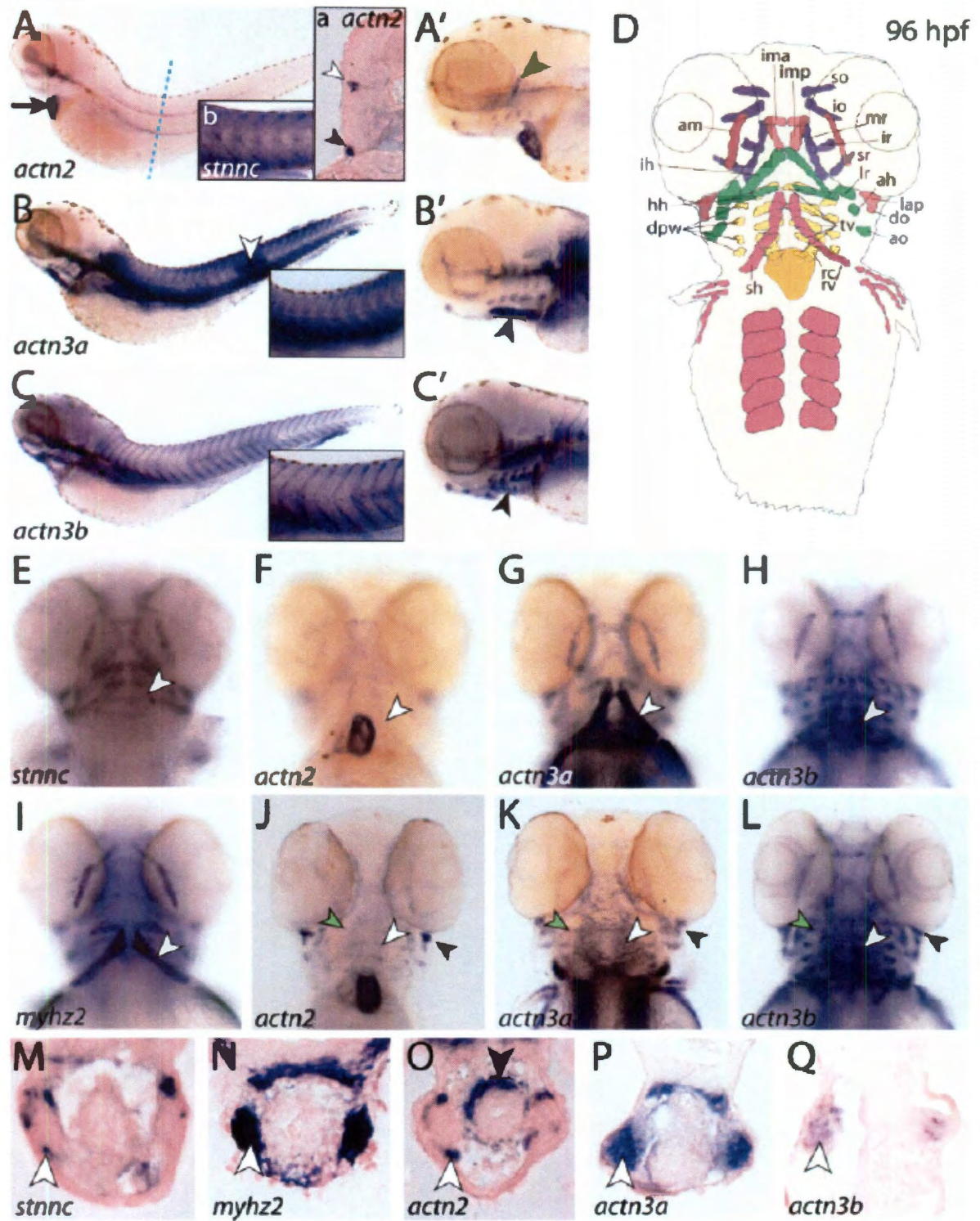


Figure 4.4. (Legend on following pages.)

**Figure 4.4.** (Previous page.) Muscle-specific actinins are differentially expressed in axial and craniofacial musculature at 96 hpf. A-C: lateral whole mount views. Inset Aa: transverse section at the posterior gut level; insets Ab, B and C are higher magnification lateral views of somite expression. A'-C': higher magnification lateral views of craniofacial expression from A-C. D: camera lucida representation identifying muscles of zebrafish at 96hpf (abbreviations listed in Table 1). E-I, F'-H': Ventral views of craniofacial expression, with E-I having a ventral focal plane and F'-H' being more a dorsal focal plane. Jaw structures and sternohyoideus muscles have been removed in G' for visibility of more dorsal muscles. J-N: Transverse sections at the level of the heart. **A,A'**: Expression of *actn2* at 96 hpf. Expression is seen in the heart (arrow) as well as the lateralis superficialis (white arrowhead) and inferior obliquus (black arrowhead). In the cranial musculature, strong *actn2* expression was seen in lap muscles (green arrowhead). Inset **Ab** shows broad expression of *stnnc* at 96 hpf in the slow fibers of the myotome. **B&B'**: Expression of *actn3a* at 96 hpf. Expression was seen in the axial musculature (white arrowhead, superficial expression). Expression was also seen in cranial and pharyngeal muscles and strong expression is seen in the sh (arrowhead). **C&C'**: Expression of *actn3b* at 96 hpf. Expression was seen in the axial musculature. Weak expression was seen in the sh (arrowhead). **D**: Craniofacial muscle groups are colored to demarcate pharyngeal arches of origin: red, mandibular arch (pharyngeal arch 1, P1); green, hyoid arch (P2); yellow, branchial arches 1-5 (P3-P7);

**Figure 4.4** (legend continued) purple, extraocular/cranial muscle; pink, somite-derived muscle; orange, cardiac muscle. **E:** *stnnc* was expressed uniformly in most cranial and pharyngeal muscle. Expression was light in sh muscles (white arrowhead). **F-H:** Expression of the muscle-specific actinins in sh muscles was variable between homologs. *actn2* was weakly expressed in the sh (arrowhead, F), *actn3a* was very strongly expressed (arrowhead, G), and *actn3b* was moderately expressed (arrowhead, H). **I:** *myhz2* was expressed strongly in sh muscles (arrowhead). **J:** *actn2* expression was weak in tv and dpw muscles (white and green arrowheads, respectively) compared to its strong expression in lap muscles (black arrowhead). **K&L:** *actn3a* (K) was weakly expressed in tv (white arrowheads), dpw (green arrowheads) and lap (black arrowheads) muscle pairs. *actn3b* (L) expression was high in all pharyngeal muscles. **M-Q:** *stnnc* was expressed in the periphery of the sh (arrowhead, M). *myhz2* was expressed in the center of the sh (arrowhead, N). *actn2* was expressed in the periphery of the sh (arrowhead, O). *actn3a* was expressed in the center of the sh (arrowhead, P). *actn3b* was expressed in the center of the sh (arrowhead, Q).

patches of expression (Fig. 4.4B). These patches were located in the trunk and anterior tail from multiple clutches and may indicate transient high level expression of *actn3* genes.

#### **4.8 Muscle actinins display different patterns of expression in the pharyngeal and cranial muscles.**

We examined the expression of the muscle actinins in the cranial and pharyngeal musculature of 96 hpf zebrafish (Table 4.1, Fig. 4.4). These embryonic muscles have been shown to be composed of slow and fast muscle and are thought to maintain similar morphology and function as their adult forms (Winterbottom, 1973). These muscles are likely to have diverse physiological specializations for their specific functions.

#### **4.9 Differential expression of *actn2* in mandibular and hyoid arches**

We observed low levels of *actn2* in most muscles (Table 4.1). However, one exception to this was the levator arcus palatine (lap) muscle, a predominant muscle associated with compression of the buccal cavity and opercula (Hernández, 2000; Winterbottom, 1973). This muscle is responsible for constant perfusion of oxygenated water over respiratory gills, and expressed *actn2* strongly (Fig 4.4J). Interestingly, the largest differences in expression between *actn2* and both *actn3* paralogs were observed in the lateral muscles of Arch I and Arch II, the mandibular and hyoid arches, respectively. More specifically, all three cases of decreased *actn2* expression

relative to the other muscle actinins were in muscles associated with either mandibular closing or opercula movement. The dilator opercula functions to withdraw, or open, the operculum while adductor mandibulae muscles are responsible for the forced, medial closure of the mandibular cartilages. In the mandibular arch, adductor mandibulae and dilator operculi muscles showed markedly less expression of *actn2* than either *actn3* gene (Table 4.1, Fig 4.4F-H&J-L).

#### **4.10 Differential expression of *actn3* paralogs in branchial arches and somite-derived anterior muscles**

With one exception, we observed large differences between *actn3a* and *actn3b* expression within the five branchial arches (pharyngeal arches three through seven). Specifically, *actn3b* was the dominant *actn3* paralog expressed in transversus ventralis and dorsal pharyngeal wall muscle pairs. While *actn3a* staining was observed in these muscles, it was reduced (Fig 4.4K&L). The transversus ventralis muscles insert on ceratobranchial cartilages and control gill bar movements while the dorsal pharyngeal wall muscles insert on the lateral and dorsal edges of the branchial arches and expand the buccal chamber (Hernandez et al., 2005).

Conversely, *actn3a* was observed to be the preferred *actn3* paralog expressed in sternohyoideus muscles at 96 hpf (Fig 4.4G&H). The sternohyoideus muscles are derived from somitic mesoderm, which migrates anteriorly and inserts into hyoidal cartilages (Huang et al., 1999; Schilling and

Kimmel, 1997; Winterbottom, 1973). The sternohyoideus muscles have been shown to express predominantly fast muscle fibers throughout larval development and are the dominant muscles that rapidly open the hyoid jaw during feeding (Hernandez et al., 2005).

Region		Muscle	<i>actn2</i>	<i>actn3a</i>	<i>actn3b</i>
mandibular arch	am	adductor mandibulae	+	++	+++
	do	dilator operculi	+	++	+++
	ima	intermandibularis anterior	+/-	+	++
	imp	intermandibularis posterior	+/-	+/-	-
	lap	levator arcus palatini	+++	+++	+++
hyoid arch	ah	adductor hyoideus	++	++	+++
	ao	adductor operculi	+	+++	+++
	hh	hyohyoideus	+/-	+	++
	ih	interhyoideus	+/-	+/-	+
	lo	levator operculi	n/a	n/a	n/a
branchial arches	dpw	dorsal pharyngeal wall 1-5	+	+	+++
	rc	rectus communis	n/a	n/a	n/a
	rv	rectus ventralis	n/a	n/a	n/a
	tv	transversus ventralis 1-5	++	+	+++
extraocular	io	inferior oblique	+	+/-	+
	ir	inferior rectus	-	+/-	-
	lr	lateral rectus	++	++	+++
	mr	medial rectus	+	+	+/-
	so	superior oblique	+	+/-	+
	sr	superior rectus	+	++	+
somite	sh	sternohyoideus	+/-	+++	+

**Table 4.1** Relative expression of muscle actinins in 96 hpf cranial and pharyngeal muscles. Color of region corresponds to Fig5.4D. Locations of muscles are indicated by their abbreviations in Figure 5.4G. Expression levels are identified as: n/a not analyzed, - no expression, +/- weak variable expression, + weak consistent expression, ++ moderate expression, +++ strong expression.

#### 4.11 Expression of *actn2*, *3a* and *3b* in the sternohyoideus muscles

The cranial and pharyngeal muscles have segregated populations of slow and fast muscle fibers with slow muscle fibers surrounding the central fast muscle fibers (Diogo et al., 2008). In order to determine if the zebrafish actinins are restricted to slow- or fast-specific domains of these muscles, the expression of the muscle-specific actinin genes was analyzed by sectioning the large, easily identified 96 hpf sternohyoideus muscles. We used *stnnc* as a marker for slow fibers and *myhz2* as a fast fiber marker. *actn2* was expressed in a small number of cells restricted to the outside of the bundle of fibers composing the sternohyoideus muscle (Fig. 4.4O). This pattern appears to be identical to the slow muscle fibers expressing *stnnc* (Fig. 4.4M). Thus, at least in the case of this muscle, *actn2* expression is restricted to the slow muscle cell population. In contrast to the peripheral punctate expression of *actn2*, both *actn3a* and *actn3b* are expressed in many of the fibers of the sternohyoideus (Fig 4.4P&Q). As described above, *actn3a* expression was much greater than *actn3b* in these muscles.

These differences in expression patterns within muscles of the head and pharynx indicate diversification of gene expression associated with specific muscles. The complement of actinins expressed in different muscle fibers may direct their contractile or physiological properties. Muscles associated with feeding require fast, strong contractions, while those associated with respiration require slower and more regular contractions. Also, differential regulation of the actinins may reflect a difference in



embryological origin and subfunctionalization of the duplicated *actn3a* and *actn3b* in lineages that have different origins. However, one of the differences we have described between expression of the *actn3* paralogs is in the transversus ventralis, while other muscles derived from the same arch maintain similar expression of both paralogs. The changes could also be associated with neofunctionalization and expression in teleost specific muscles. However, we do not see differences in the teleost specific intermandibularis posterior or interhyodeus (Mills et al., 2001; North and Beggs, 1996).

#### **4.12 Conclusion**

This work is the first comprehensive examination of alpha-actinin expression in vertebrates. We have used a bioinformatics approach to identify members of the *alpha-actinin* gene family in the zebrafish genome. We identified clear orthologs of all identified mammalian actinin genes, including two splice isoforms of *actn1* homologous to those described for human *ACTN1*. We also identified two paralogs of human *ACTN3*. We characterized the temporal profile of expression of each family member through 8 days of zebrafish development. By whole mount *in situ* hybridization we observed that the widespread expression of *actn1* was conserved. We observed that the onset of unique and restricted expression domains of the muscle-specific actinins corresponded to the onset of muscle

differentiation, and that each of the three genes had distinct expression patterns.

Muscle-specific actinins display different expression patterns in different vertebrates. In humans, *ACTN2* is expressed in all skeletal muscle fibers, with *ACTN3* restricted to a subset of Type II (fast) fibers (Taylor et al., 2003; Volff, 2005; Woods et al., 2005). Chickens do not have an *actn3* gene, nor could we identify any other avian *actn3* sequences (data not shown). In zebrafish *actn2* is transiently expressed in axial slow muscle, but is then down regulated in most slow muscle cells of the trunk and tail. In cranial and pharyngeal muscles the relative levels of *actn2* vary, with strong expression in the levator operculi but not in other muscles. Sections of the sternohyoidus muscle indicated that *actn2* is restricted to the slow muscle fiber compartment of this muscle. We tentatively conclude that *actn2* expression is restricted to a subset of slow muscle fibers in many muscles. However a more comprehensive analysis is required to support this conclusion. Zebrafish *actn3a* and *actn3b* are the dominantly-expressed muscle actinins, and one or the other are expressed throughout the developing musculature. The overlapping but distinct expression patterns of the *actn3* genes indicate that there may be functional differences between the two genes that arose in duplicated *actn3* genes following the teleost genome duplication (Taylor et al., 2003; Volff, 2005; Woods et al., 2005). However, we searched the current genome assemblies of medaka (HdrR) and stickleback (BROAD S1) and found only a single *actn3* gene in either genome (data not shown). This

indicates that the retention of *actn3* duplicates may not be widespread in teleosts, and that the differences may represent subfunctionalization of the *actn3* genes in zebrafish and a unique requirement for non-overlapping domains resulting in the maintenance of both *actn3* paralogs. The presence of duplicated *actn3* genes in zebrafish is in direct contrast to the absence of functional ACTN3 in many humans and chickens. Neither humans nor mice nor chickens require ACTN3 for viability, and loss of ACTN3 is associated with changes in muscle performance (MacArthur et al., 2007; Yang et al., 2003; North et al., 1999).

In contrast to the differences in Actn3, we observed striking conservation in the Actn1 isoforms in zebrafish and humans, including conservation of the calcium insensitive isoform c. The conservation of some members of this family and divergence of others indicates that the functions of actinins are diverse. The zebrafish will be an exciting platform for investigation of the roles that the actinins play in development, disease and evolution.

## Chapter 5: Discussion

### 5.1 *pwg* regulates YSL integrity during morphogenesis

The *pwg* mutant phenotype arises from the requirement for the yolk cell to direct development of the embryo. Map3K4 is required to maintain yolk cell integrity. 24 hpf *pwg* mutant embryos suffered fragmented YSN resulting from rapid collapse of YSL integrity at the time when the phenotype begins to manifest in the overlying blastoderm. At later stages of development during organogenesis, affected embryos show characteristic loss of ECM components that require signals from the yolk for their expression and deposition (Arrington and Yost, 2009; Sakaguchi et al., 2006; Trinh and Stainier, 2004).

I have shown that *pwg* is required in the yolk during early development for normal axial mesoderm extension and for dorsal convergence of the overlying neurectoderm of the anterior neural plate. In mutant embryos, the chordamesoderm, prechordal plate, neural and non-neural ectoderm, and the midbrain-hindbrain boundary are correctly specified during gastrulation, however later morphogenetic events are affected, coinciding with the timing of yolk cell failure. I hypothesize that the constriction of the YSL that occurs in *pwg* has the same underlying defect as *bbp* mutants and that the differences in phenotype are due to differences in timing and requirement for specific yolk cell functions at different times of development. Supporting this hypothesis, we have observed *bbp* escapers, all of which display *pwg* phenotype at 24 hpf (SGdITC and DSW unpublished observations).

## 5.2 Conditional interactions between *map3k4*, *mxtx1* and *fibronectin*

*pwg* encodes a hypomorphic allele of *map3k4*, a mitogen-activated protein kinase kinase kinase upstream of p38 MAPK and MK2. I also highlight a genetic interaction between MAPK signaling and *mxtx1*, where disrupting the activity of both in the YSL greatly increases the penetrance of the *pwg* phenotype. Previous reports have shown that *mxtx1* is involved in ECM gene expression and have proposed that a maternal factor could regulate the expression or function of *mxtx1* in the YSL (Hirata et al., 2000; Sakaguchi et al., 2006).

Our data presented here do not support a role for *map3k4* regulating *mxtx1* expression. However, *mxtx1* clearly plays a role in YSL stability during development, since morpholino-mediated knockdown of *mxtx1* in *pwg* mutants greatly increases the mutant phenotype penetrance and *mxtx1* RNA can rescue the *pwg* phenotype. This indicates that Map3k4 may regulate the activity but not expression of Mxtx1. Regulation of Mxtx1 activity may explain the lack of interaction between *pwg* and *fn1*. It is likely that wild type embryos from *pwg* mutant females have sufficient Mxtx1 activity to prevent an interaction with *fn1*. Unfortunately, because *pwg* is a hypomorphic allele, clear interpretation of epistasis is not possible, leaving open the possibility that Mxtx1 acts upstream of Map3k4 to promote its function.

The specific and reproducible defects in embryonic morphogenesis observed during segmentation following yolk cell collapse indicate that a

specific yolk cell function dominates during this time. Defective ECM deposition is an attractive model for this function. The earliest sites of ECM deposition form at the interface of the hypoblast and yolk and between the epiblast and hypoblast tissues during gastrulation and late gastrulation and segmentation stages are likely the time of the first strict requirement for ECM dependent morphogenetic processes (Arrington and Yost, 2009; Latimer and Jessen, 2010; Trinh and Stainier, 2004). It is possible that the epiblast and hypoblast lose cohesion due to lack of ECM deposition and fibrils between these two domains in *pwg* mutant embryos and/or *mxtx1* morphants, causing the prechordal plate to lose contact with the overlying epiblast and buckle into the yolk. Additionally, regulation and recycling of adhesion molecules in the migrating mesoderm is an important component of vertebrate gastrulation (Kane et al., 2005; Marsden and DeSimone, 2003; Solnica-Krezel, 2006). Defects in ECM deposition resulting from knockdown of MAPK signaling or *mxtx1* activity in the yolk could impact the efficacy of cell adhesion elements at the yolk-blastoderm interface.

### **5.3 The role of the YSL during morphogenesis**

The precise correlation of the catastrophic *pwg* YSN phenotype with abnormal embryo morphogenesis at 24 hpf, indicates that the primary defect in *pwg* mutants is related to YSL integrity. In such a model, the morphogenetic defects observed in the overlying blastoderm of *pwg* embryos are caused by the absence of any coherent support or instruction from the

YSL after its collapse. Embryos that don't undergo YSL catastrophe are able to develop normally, while mutant embryos without a functional YSL have deformed morphology at 24 hpf. Dependence of embryonic morphogenesis on YSL integrity would explain the partially penetrant but fully expressed "all or nothing" phenotype of *pwg* mutants.

In addition to defects resulting from loss of ECM, the biomechanical integrity of the yolk cell itself is likely to be important for morphogenesis, providing resistance for the morphogenetic movements of the overlying blastoderm. The YSL likely has an important role in maintaining, responding or possibly even creating the required biomechanical forces that allow for the radical reorganization of the blastoderm during gastrulation. In fact, p38 MAPK activation has been previously associated with response to dynamic mechanical environments in the mammalian heart and vasculature (Kerkelä et al., 2002; Liu et al., 2008). Supporting this hypothesis is our observation of plunging prechordal plates in *pwg* mutants, where the lack of a structural support provided by the YSL underneath the migrating axial tissue might allow for buckling. This resulting axial mesoderm defect could potentially disrupt timing or location of signal transduction to the overlying anterior epiblast in these embryos (Chuang and Raymond, 2002; Tallafuss et al., 2003; Varga et al., 1999), or the defective yolk cell may fail to provide a sufficiently stiff substrate for elevation of the anterior neural tube during neurulation.

Our results underscore the critical importance of the extra-embryonic YSL during morphogenesis of the zebrafish embryo. These results build on our previous results demonstrating that the p38 MAPK pathway is a critical regulator of the yolk cell cytoskeleton (Holloway et al., 2009) and demonstrate that this pathway continues to function after 50% epiboly to maintain the yolk cell. Future work on the function of the p38 MAPK pathway in this unique cell will reveal fundamental principles of p38 MAPK activity in diverse biological processes.

#### **5.4 Future work**

Much of the remaining work involves identifying the precise cell behaviors that are disrupted in *pwg* mutant embryos. Time lapse movies and fluorescent imaging of cells of the prechordal plate will allow us to determine if cellular processes of the anterior cells of the prechordal plate are affected in *pwg* and p38a-compromized embryos. The cells at the leading edge of the prechordal plate as well as lateral cell populations that converge dorsally have specialized actin-based cell motility as well as adhesive characteristics (Kai et al., 2008). It is possible that the convergence and extension defects observed in the *pwg* and p38-compromised embryos result from failure to form filapodia or lamellipodia, or extend these cellular processes in the correct axis of migration, or to maintain these processes for a long enough duration to effect cell motility, or a combination of these. I could also scatter label embryos using a membrane-GFP construct to quantify cellular



protrusions in individual cells. Fluorophore uncaging experiments using a CMNB-fluorescein at the onset of gastrulation could allow for quantification of defects in axial and lateral mesoderm and ectoderm convergence and extension behaviors in *pwg* embryos.

Even if the data continue to support a model whereby Map3k4 and Mxtx1 have a primary function in the YSL, these blastoderm cell behavior assays are still of fundamental importance. No system in the literature describes the precocious elimination of the YSL after gastrulation, and understanding which tissues in the blastoderm rely on signals or adherence to the YSL has the potential to provide insight into role during morphogenesis.

There are several other interesting candidate genes to examine for their interaction with the *pollywog* phenotype. Filamin A/Actin Binding Protein-280 in particular has been shown to be unregulated in Map3k4 knockout mice forebrains, leading to over-stabilization of Actin stress fiber and Filamin A complexes, retarding neuronal migration (Sarkisian et al., 2006). Since Map3k4 facilitates neuronal migration by turnover of Filamin A in the mouse system, over-expression of this gene in the YSL might phenocopy *pollywog* by creating abnormally stiff or rigid areas in the YSL. Also, as mentioned above in the background section, Syndecan 2 is required for Fibronectin-mediated cardiac precursor migration and Fibronectin fibrillogenesis during development. A dominant negative Syndecan 2 construct injected into the YSL would allow us to examine a possible interaction with *pwg* mutants or ECM components.

The missense mutation in *pwg* mutants creates a YFLQ primary sequence predicted to be recognized by the SH2 domain of Stat3 (Fig 12, Human Protein Reference Database). The *pwg* mutation lies in a conserved region of the *map3k4* dimerization domain. One possibility that could be examined is that Stat3 is erroneously binding to the *pwg* Map3k4 protein and not allowing it to homodimerize and activate its downstream targets. Using site directed mutagenesis to change the tyrosine encoded in *pwg* mutants to a serine which should retain its ability to be externally oriented at the hydrophilic cytoplasmic face while also eliminating the possible Stat3-SH2 binding site. Expression of this new *map3k4* allele may be capable of rescuing *pwg* mutant embryos with the same efficacy as wild type Map3k4, which would implicate ectopic Stat3 binding to the mutated Map3k4 as a possible mechanism for the *pwg* phenotype.

## Chapter 6: Works Cited

- Abell AN, Rivera-Perez JA, Cuevas BD, Uhlik MT, Sather S, Johnson NL, Minton SK, Lauder JM, Winter-Vann AM, Nakamura K, Magnuson T, Vaillancourt RR, Heasley LE, Johnson GL. 2005. Ablation of MEKK4 kinase activity causes neurulation and skeletal patterning defects in the mouse embryo. *Mol Cell Biol* 25:8948-8959.
- Akimenko M-A, Ekker M, Wegner J, Lin W, Westerfield M. 1994. Combinatorial expression of three zebrafish genes related to distal-less: Part of a homeobox gene code for the head. *Journal of Neuroscience* 14:3475-3486.
- Arimura C, Suzuki T, Yanagisawa M, Imamura M, Hamada Y, Masaki T. 1988. Primary structure of chicken skeletal muscle and fibroblast alpha-actinins deduced from cDNA sequences. *Eur J Biochem* 177:649-55.
- Arrington CB, Yost HJ. 2009. Extra-embryonic syndecan 2 regulates organ primordia migration and fibrillogenesis throughout the zebrafish embryo. *Development* 136:3143-3152.
- Beggs AH, Byers TJ, Knoll JH, Boyce FM, Bruns GA, Kunkel LM. 1992. Cloning and characterization of two human skeletal muscle alpha-actinin genes located on chromosomes 1 and 11. *J Biol Chem* 267:9281-8.
- Bischof J, Driever W. 2004. Regulation of hhex expression in the yolk syncytial layer, the potential Nieuwkoop center homolog in zebrafish. *Dev Biol* 276:552-562.
- Blagden CS, Currie PD, Ingham PW, Hughes SM. 1997. Notochord induction of zebrafish slow muscle mediated by Sonic hedgehog. *Genes Dev* 11:2163-75.
- Bruce AE, Howley C, Dixon Fox M, Ho RK. 2005. T-box gene eomesodermin and the homeobox-containing Mix/Bix gene mtx2 regulate epiboly movements in the zebrafish. *Dev Dyn* 233:105-14.
- Burridge K, Feramisco JR. 1981. Non-muscle alpha actinins are calcium-sensitive actin-binding proteins. *Nature* 294:565-7.
- Carvalho L, Heisenberg C-P. 2010. The yolk syncytial layer in early zebrafish development. *Trends Cell Biol*.  
<http://www.ncbi.nlm.nih.gov/pubmed/20674361>.
- Catchen JM, Conery JS, Postlethwait JH. 2009. Automated identification of conserved synteny after whole-genome duplication. *Genome Res* 19:1497-1505.
- Chan Y, Tong HQ, Beggs AH, Kunkel LM. 1998. Human skeletal muscle-specific alpha-actinin-2 and -3 isoforms form homodimers and heterodimers in vitro and in vivo. *Biochem Biophys Res Commun* 248:134-9.
- Chen S, Kimelman D. 2000. The role of the yolk syncytial layer in germ layer patterning in zebrafish. *Development* 127:4681-4689.

- Chi H, Sarkisian MR, Rakic P, Flavell RA. 2005. Loss of mitogen-activated protein kinase kinase 4 (MEKK4) results in enhanced apoptosis and defective neural tube development. *Proc Natl Acad Sci USA* 102:3846-3851.
- Chowrashi P, Mittal B, Sanger JM, Sanger JW. 2002. Amorphin is phosphorylase; phosphorylase is an alpha-actinin-binding protein. *Cell Motil Cytoskeleton* 53:125-35.
- Chuang JC, Raymond PA. 2002. Embryonic origin of the eyes in teleost fish. *Bioessays* 24:519-529.
- Costa ML, Escaleira R, Manasfi M, de Souza LF, Mermelstein CS. 2003. Cytoskeletal and cellular adhesion proteins in zebrafish (*Danio rerio*) myogenesis. *Braz J Med Biol Res* 36:1117-1120.
- Costa ML, Escaleira RC, Rodrigues VB, Manasfi M, Mermelstein CS. 2002. Some distinctive features of zebrafish myogenesis based on unexpected distributions of the muscle cytoskeletal proteins actin, myosin, desmin, alpha-actinin, troponin and titin. *Mech Dev* 116:95-104.
- Craig EA, Stevens MV, Vaillancourt RR, Camenisch TD. 2008. MAP3Ks as central regulators of cell fate during development. *Dev Dyn* 237:3102-3114.
- D'Amico LA, Cooper MS. 2001. Morphogenetic domains in the yolk syncytial layer of axiating zebrafish embryos. *Dev Dyn* 222:611-624.
- Devoto SH, Melançon E, Eisen JS, Westerfield M. 1996. Identification of separate slow and fast muscle precursor cells in vivo, prior to somite formation. *Development* 122:3371-80.
- Diogo R, Hinits Y, Hughes SM. 2008. Development of mandibular, hyoid and hypobranchial muscles in the zebrafish: homologies and evolution of these muscles within bony fishes and tetrapods. *BMC Developmental Biology* 8:24.
- Dosch R, Wagner DS, Mintzer KA, Runke G, Wiemelt AP, Mullins MC. 2004. Maternal control of vertebrate development before the midblastula transition: mutants from the zebrafish I. *Dev Cell* 6:771-780.
- Draper BW, Morcos PA, Kimmel CB. 2001. Inhibition of zebrafish *fgf8* pre-mRNA splicing with morpholino oligos: a quantifiable method for gene knockdown. *Genesis* 30:154-156.
- Driever W, Solnica-Krezel L, Schier AF, Neuhauss SC, Malicki J, Stemple DL, Stainier DY, Zwartkuis F, Abdelilah S, Rangini Z, Belak J, Boggs C. 1996. A genetic screen for mutations affecting embryogenesis in zebrafish. *Development* 123:37-46.
- Elworthy S, Hargrave M, Knight R, Mebus K, Ingham PW. 2008. Expression of multiple slow myosin heavy chain genes reveals a diversity of zebrafish slow twitch muscle fibres with differing requirements for Hedgehog and *Prdm1* activity. *Development* 135:2115-2126.
- Frey N, Olson EN. 2002. Calsarcin-3, a novel skeletal muscle-specific member of the calsarcin family, interacts with multiple Z-disc proteins. *J Biol Chem* 277:13998-4004.

- Garavito-Aguilar ZV, Riley HE, Yelon D. 2010. Hand2 ensures an appropriate environment for cardiac fusion by limiting Fibronectin function. *Development*. <http://www.ncbi.nlm.nih.gov/pubmed/20724450>.
- Geeves MA, Holmes KC. 1999. Structural mechanism of muscle contraction. *Annu Rev Biochem* 68:687-728.
- Haffter P, Granato M, Brand M, Mullins MC, Hammerschmidt M, Kane DA, Odenthal J, van Eeden FJ, Jiang YJ, Heisenberg CP, Kelsh RN, Furutani-Seiki M, Vogelsang E, Beuchle D, Schach U, Fabian C, Nüsslein-Volhard C. 1996. The identification of genes with unique and essential functions in the development of the zebrafish, *Danio rerio*. *Development* 123:1-36.
- Haiech J, Kilhoffer MC, Lukas TJ, Craig TA, Roberts DM, Watterson DM. 1991. Restoration of the calcium binding activity of mutant calmodulins toward normal by the presence of a calmodulin binding structure. *Journal of Biological Chemistry* 266:3427-3431.
- Hammerschmidt M, Pelegri F, Mullins MC, Kane DA, Brand M, van Eeden FJ, Furutani-Seiki M, Granato M, Haffter P, Heisenberg CP, Jiang YJ, Kelsh RN, Odenthal J, Warga RM, Nusslein-Volhard C. 1996. Mutations affecting morphogenesis during gastrulation and tail formation in the zebrafish, *Danio rerio*. *Development* 123:143-51.
- Hernández LP. 2000. Intraspecific scaling of feeding mechanics in an ontogenetic series of zebrafish, *Danio rerio*. *J Exp Biol* 203:3033-43.
- Hernandez LP, Patterson SE, Devoto SH. 2005. The development of muscle fiber type identity in zebrafish cranial muscles. *Anatomy and Embryology* 209:323-334.
- Hirata T, Yamanaka Y, Ryu SL, Shimizu T, Yabe T, Hibi M, Hirano T. 2000. Novel mix-family homeobox genes in zebrafish and their differential regulation. *Biochem Biophys Res Commun* 271:603-609.
- Holloway BA, Gomez de la Torre Canny S, Ye Y, Slusarski DC, Freisinger CM, Dosch R, Chou MM, Wagner DS, Mullins MC. 2009. A novel role for MAPKAPK2 in morphogenesis during zebrafish development. *PLoS Genet* 5:e1000413.
- Hollway GE, Currie PD. 2003. Myotome meanderings. Cellular morphogenesis and the making of muscle. *EMBO reports* 4:855.
- Holterhoff CK, Saunders RH, Brito EE, Wagner DS. 2009. Sequence and expression of the zebrafish alpha-actinin gene family reveals conservation and diversification among vertebrates. *Dev Dyn* 238:2936-2947.
- Janssen KP, Eichinger L, Janmey PA, Noegel AA, Schliwa M, Witke W, Schleicher M. 1996. Viscoelastic properties of F-actin solutions in the presence of normal and mutated actin-binding proteins. *Arch Biochem Biophys* 325:183-9.
- Kai M, Heisenberg C-P, Tada M. 2008. Sphingosine-1-phosphate receptors regulate individual cell behaviours underlying the directed migration of prechordal plate progenitor cells during zebrafish gastrulation. *Development* 135:3043-3051.

- Kane DA, Hammerschmidt M, Mullins MC, Maischein HM, Brand M, van Eeden FJ, Furutani-Seiki M, Granato M, Haffter P, Heisenberg CP, Jiang YJ, Kelsh RN, Odenthal J, Warga RM, Nusslein-Volhard C. 1996. The zebrafish epiboly mutants. *Development* 123:47-55.
- Kane DA, McFarland KN, Warga RM. 2005. Mutations in half baked/E-cadherin block cell behaviors that are necessary for teleost epiboly. *Development* 132:1105-16.
- Kaplan JM, Kim SH, North KN, Rennke H, Correia LA, Tong HQ, Mathis BJ, Rodríguez-Pérez JC, Allen PG, Beggs AH, Pollak MR. 2000. Mutations in ACTN4, encoding alpha-actinin-4, cause familial focal segmental glomerulosclerosis. *Nat Genet* 24:251-6.
- Kawahara A, Nishi T, Hisano Y, Fukui H, Yamaguchi A, Mochizuki N. 2009. The sphingolipid transporter spns2 functions in migration of zebrafish myocardial precursors. *Science* 323:524-527.
- Kerkelä R, Pikkarainen S, Majalahti-Palviainen T, Tokola H, Ruskoaho H. 2002. Distinct roles of mitogen-activated protein kinase pathways in GATA-4 transcription factor-mediated regulation of B-type natriuretic peptide gene. *J Biol Chem* 277:13752-13760.
- Kimelman D, Schier AF. 2002. Mesoderm induction and patterning. *Results Probl Cell Differ* 40:15-27.
- Kimmel CB, Ballard WW, Kimmel SR, Ullmann B, Schilling TF. 1995. Stages of embryonic development of the zebrafish. *Dev Dyn* 203:253-310.
- Krauss S, Concordet J-P, Ingham PW. 1993. A functionally conserved homolog of the Drosophila segment polarity gene hh is expressed in tissues with polarizing activity in zebrafish embryos. *Cell* 75:1431-1444.
- Krauss S, Maden M, Holder N, Wilson SW. 1992. Zebrafish pax[b] is involved in the formation of the midbrain-hindbrain boundary. *Nature* 360:87-89.
- Latimer A, Jessen JR. 2010. Extracellular matrix assembly and organization during zebrafish gastrulation. *Matrix Biol* 29:89-96.
- Lee KH, Xu Q, Breitbart RE. 1996. A new tinman-related gene, nkx2.7, anticipates the expression of nkx2.5 and nkx2.3 in zebrafish heart and pharyngeal endoderm. *Dev Biol* 180:722-731.
- Li Y, Allende ML, Finkelstein R, Weinberg ES. 1994. Expression of two zebrafish orthodenticle-related genes in the embryonic brain. *Mech Dev* 48:229-244.
- Liu B, Qu M-J, Qin K-R, Li H, Li Z-K, Shen B-R, Jiang Z-L. 2008. Role of cyclic strain frequency in regulating the alignment of vascular smooth muscle cells in vitro. *Biophys J* 94:1497-1507.
- MacArthur DG, Seto JT, Raftery JM, Quinlan KG, Huttley GA, Hook JW, Lemckert FA, Kee AJ, Edwards MR, Berman Y, Hardeman EC, Gunning PW, Eastal S, Yang N, North KN. 2007. Loss of ACTN3 gene function alters mouse muscle metabolism and shows evidence of positive selection in humans. *Nat Genet* 39:1261-5.

- Marsden M, DeSimone DW. 2003. Integrin-ECM interactions regulate cadherin-dependent cell adhesion and are required for convergent extension in *Xenopus*. *Curr Biol* 13:1182-1191.
- Marza E, Barthe C, André M, Villeneuve L, Hérou C, Babin PJ. 2005. Developmental expression and nutritional regulation of a zebrafish gene homologous to mammalian microsomal triglyceride transfer protein large subunit. *Dev Dyn* 232:506-518.
- Michaud J-LR, Hosseini-Abardeh M, Farah K, Kennedy CRJ. 2009. Modulating alpha-actinin-4 dynamics in podocytes. *Cell Motil Cytoskeleton* 66:166-78.
- Mills MA, Yang N, Weinberger RP, Vander Woude DL, Beggs AH, Easteal S, North KN. 2001. Differential expression of the actin-binding proteins, alpha-actinin-2 and -3, in different species: implications for the evolution of functional redundancy. *Human Molecular Genetics* 10:1335-1346.
- Mita H, Tsutsui J, Takekawa M, Witten EA, Saito H. 2002. Regulation of MTK1/MEKK4 kinase activity by its N-terminal autoinhibitory domain and GADD45 binding. *Mol Cell Biol* 22:4544-4555.
- Miyake Z, Takekawa M, Ge Q, Saito H. 2007. Activation of MTK1/MEKK4 by GADD45 through induced N-C dissociation and dimerization-mediated trans autophosphorylation of the MTK1 kinase domain. *Mol Cell Biol* 27:2765-2776.
- Mizuno T, Yamaha E, Wakahara M, Kuroiwa A, Takeda H. 1996. Mesoderm induction in zebrafish. *Nature* 383:131-132.
- Montero JA, Carvalho L, Wilsch-Brauninger M, Kilian B, Mustafa C, Heisenberg CP. 2005. Shield formation at the onset of zebrafish gastrulation. *Development* 132:1187-98.
- Montero JA, Heisenberg CP. 2004. Gastrulation dynamics: cells move into focus. *Trends Cell Biol* 14:620-7.
- North KN, Beggs AH. 1996. Deficiency of a skeletal muscle isoform of alpha-actinin (alpha-actinin-3) in merosin-positive congenital muscular dystrophy. *Neuromuscul Disord* 6:229-35.
- North KN, Yang N, Wattanasirichaigoon D, Mills M, Easteal S, Beggs AH. 1999. A common nonsense mutation results in alpha-actinin-3 deficiency in the general population. *Nat Genet* 21:353-4.
- Ober EA, Schulte-Merker S. 1999. Signals from the yolk cell induce mesoderm, neuroectoderm, the trunk organizer, and the notochord in zebrafish. *Dev Biol* 215:167-181.
- Ochi H, Westerfield M. 2007. Signaling networks that regulate muscle development: lessons from zebrafish. *Dev Growth Differ* 49:1-11.
- Ono Y, Liang C, Ikeda D, Watabe S. 2006. cDNA cloning of myosin heavy chain genes from medaka *Oryzias latipes* embryos and larvae and their expression patterns during development. *Developmental Dynamics* 235.
- Osborne N, Brand-Arzamendi K, Ober EA, Jin S-W, Verkade H, Holtzman NG, Yelon D, Stainier DYR. 2008. The spinster homolog, two of hearts,

- is required for sphingosine 1-phosphate signaling in zebrafish. *Curr Biol* 18:1882-1888.
- Otey CA, Carpen O. 2004.  $\alpha$ -Actinin revisited: a fresh look at an old player. *Cell motility and the cytoskeleton* 58.
- Parsons MJ, Pollard SM, Saúde L, Feldman B, Coutinho P, Hirst EMA, Stemple DL. 2002. Zebrafish mutants identify an essential role for laminins in notochord formation. *Development* 129:3137-3146.
- Pelegri F, Schulte-Merker S. 1999. A gynogenesis-based screen for maternal-effect genes in the zebrafish, *Danio rerio*. *Methods Cell Biol* 60:1-20.
- Peng M-Y, Wen H-J, Shih L-J, Kuo C-M, Hwang S-PL. 2002. Myosin heavy chain expression in cranial, pectoral fin, and tail muscle regions of zebrafish embryos. *Mol Reprod Dev* 63:422-429.
- Rodriguez TA, Srinivas S, Clements MP, Smith JC, Beddington RSP. 2005. Induction and migration of the anterior visceral endoderm is regulated by the extra-embryonic ectoderm. *Development* 132:2513-2520.
- Sakaguchi T, Kikuchi Y, Kuroiwa A, Takeda H, Stainier DYR. 2006. The yolk syncytial layer regulates myocardial migration by influencing extracellular matrix assembly in zebrafish. *Development* 133:4063-4072.
- Sanger JW, Wang J, Holloway B, Du A, Sanger JM. 2009. Myofibrillogenesis in skeletal muscle cells in zebrafish. *Cell Motil Cytoskeleton* 66:556-566.
- Sarkisian MR, Bartley CM, Chi H, Nakamura F, Hashimoto-Torii K, Torii M, Flavell RA, Rakic P. 2006. MEKK4 signaling regulates filamin expression and neuronal migration. *Neuron* 52:789-801.
- Schilling TF, Kimmel CB. 1997. Musculoskeletal patterning in the pharyngeal segments of the zebrafish embryo. *Development* 124:2945-60.
- Schulte-Merker S, Hammerschmidt M, Beuchle D, Cho KW, De Robertis EM, Nüsslein-Volhard C. 1994. Expression of zebrafish goosecoid and no tail gene products in wild-type and mutant no tail embryos. *Development* 120:843-52.
- Serrano AL, Murgia M, Pallafacchina G, Calabria E, Coniglio P, Lømo T, Schiaffino S. 2001. Calcineurin controls nerve activity-dependent specification of slow skeletal muscle fibers but not muscle growth. *Proc Natl Acad Sci U S A* 98:13108-13.
- Solnica-Krezel L. 2006. Gastrulation in zebrafish -- all just about adhesion? *Curr Opin Genet Dev* 16:433-41.
- Solnica-Krezel L, Driever W. 1994. Microtubule arrays of the zebrafish yolk cell: organization and function during epiboly. *Development* 120:2443-55.
- Takekawa M, Posas F, Saito H. 1997. A human homolog of the yeast Ssk2/Ssk22 MAP kinase kinase kinases, MTK1, mediates stress-induced activation of the p38 and JNK pathways. *EMBO J* 16:4973-4982.



- Takekawa M, Saito H. 1998. A family of stress-inducible GADD45-like proteins mediate activation of the stress-responsive MTK1/MEKK4 MAPKKK. *Cell* 95:521-530.
- Takekawa M, Tatebayashi K, Itoh F, Adachi M, Imai K, Saito H. 2002. Smad-dependent GADD45beta expression mediates delayed activation of p38 MAP kinase by TGF-beta. *EMBO J* 21:6473-6482.
- Tallafuss A, Adolf B, Bally-Cuif L. 2003. Selective control of neuronal cluster size at the forebrain/midbrain boundary by signaling from the prechordal plate. *Dev Dyn* 227:524-535.
- Tang J, Taylor DW, Taylor KA. 2001. The three-dimensional structure of [alpha]-actinin obtained by cryoelectron microscopy suggests a model for Ca<sup>2+</sup>-dependent actin binding. *Journal of Molecular Biology* 310:845-858.
- Taylor JS, Braasch I, Frickey T, Meyer A, Van de Peer Y. 2003. Genome duplication, a trait shared by 22,000 species of ray-finned fish. *Genome Research* 13:382-390.
- Thisse C, Thisse B, Schilling TF, Postlethwait JH. 1993. Structure of the zebrafish snail1 gene and its expression in wild-type, spadetail and no tail mutant embryos. *Development* 119:1203-15.
- Thisse C, Thisse B, Halpern ME, Postlethwait JH. 1994. goosecoid Expression in neurectoderm and mesendoderm is disrupted in zebrafish cyclops gastrulas. *Developmental Biology* 164:420-429.
- Trinh LA, Stainier DYR. 2004. Fibronectin regulates epithelial organization during myocardial migration in zebrafish. *Dev Cell* 6:371-382.
- Ulrich F, Concha ML, Heid PJ, Voss E, Witzel S, Roehl H, Tada M, Wilson SW, Adams RJ, Soll DR, Heisenberg C-P. 2003. Slb/Wnt11 controls hypoblast cell migration and morphogenesis at the onset of zebrafish gastrulation. *Development* 130:5375-5384.
- Varga ZM, Wegner J, Westerfield M. 1999. Anterior movement of ventral diencephalic precursors separates the primordial eye field in the neural plate and requires cyclops. *Development* 126:5533-5546.
- Volff J-N. 2005. Genome evolution and biodiversity in teleost fish. *Heredity* 94:280-94.
- Wagner DS, Dosch R, Mintzer KA, Wiemelt AP, Mullins MC. 2004. Maternal control of development at the midblastula transition and beyond: mutants from the zebrafish II. *Dev Cell* 6:781-790.
- Weins A, Schlondorff JS, Nakamura F, Denker BM, Hartwig JH, Stossel TP, Pollak MR. 2007. Disease-associated mutant alpha-actinin-4 reveals a mechanism for regulating its F-actin-binding affinity. *Proc Natl Acad Sci U S A* 104:16080-5.
- Wilkins SJ, Yoong S, Verkade H, Mizoguchi T, Plowman SJ, Hancock JF, Kikuchi Y, Heath JK, Perkins AC. 2008. Mtx2 directs zebrafish morphogenetic movements during epiboly by regulating microfilament formation. *Dev Biol* 314:12-22.

- Winterbottom R. 1973. A Descriptive Synonymy of the Striated Muscles of the Teleostei. *Proceedings of the Academy of Natural Sciences of Philadelphia* 125:225-317.
- Witke W, Hofmann A, Köppel B, Schleicher M, Noegel AA. 1993. The Ca(2+)-binding domains in non-muscle type alpha-actinin: biochemical and genetic analysis. *J Cell Biol* 121:599-606.
- Woods IG, Wilson C, Friedlander B, Chang P, Reyes DK, Nix R, Kelly PD, Chu F, Postlethwait JH, Talbot WS. 2005. The zebrafish gene map defines ancestral vertebrate chromosomes. *Genome Res* 15:1307-1314.
- Yang N, MacArthur DG, Gulbin JP, Hahn AG, Beggs AH, Eastal S, North K. 2003. ACTN3 genotype is associated with human elite athletic performance. *Am J Hum Genet* 73:627-31.